T-4635

FEASIBILITY OF ON-BOARD CATALYTIC DECOMPOSITION OF ETHANOL FOR COLD-START ASSISTANCE

by

Jatuporn Wittayakun

T-4635

A thesis submitted to the Faculty and the Board of Trustees of the Colorado School of Mines in partial fulfillment of the requirements for the degree of Master of Science (Chemistry).

Golden, Colorado

Date 03-30-95

Signed: _____
Jatuporn Wittayakun

Approved: _____
Dr. Scott W. Cowley
Thesis Advisor

Golden, Colorado

Date 5/30/95

Approved: _____
Dr. Stephen R. Daniel
Department Head
Chemistry and Geochemistry

ABSTRACT

There are several reactions which yield hydrogen as a product. The reaction chosen for study here is the decomposition of ethanol, a renewable resource. This reaction produces methane, carbon monoxide, and hydrogen as main products. The catalysts that were used are palladium/lanthana/silica and platinum/lanthana/silica in which the silica support is covered by a thin layer of lanthana and the lanthana itself has small metal crystallites of palladium or platinum deposited on it. Since these catalysts showed high reactivity and selectivity for methanol decomposition to carbon monoxide and hydrogen (*Xu, 1992*), they were expected to have promise for the ethanol decomposition reaction. The catalysts were evaluated in a tubular flow reactor. The platinum based catalysts showed higher activity for ethanol decomposition than the palladium based catalysts. The catalyst activity increased with lanthana loading.

With 5 percent loading of lanthana, the catalyst demonstrated higher activities than 2 percent loading. However, all catalysts showed severe loss in activity during the test sequence. Catalyst coking is responsible for the activity loss.

The catalyst characterization technique used in this study was x-ray diffraction (XRD). The XRD patterns indicated that modification of silica support with lanthana improved metal dispersion in both platinum and palladium catalysts. This resulted in higher activities for the decomposition of ethanol.

TABLE OF CONTENTS

TABLE OF FIGURES

LIST OF TABLES

ACKNOWLEDGEMENTS

I would like to thank my advisor, Dr. Scott Cowley for his assistance and patience throughout this study. I would also like to thank my committee: Dr. Dean W. Dickerhoof and Dr. Stephen R. Daniel for their support.

In addition, I would like to recognize Mr. Nurak Grisdanurak ,Dr. Xianghong Zhao and my Thai friends for their help.

Finally, I wish to thank the Royal Thai Government for providing me the full financial support and for letting me continue my education in the field of my interest.

INTRODUCTION

Ethanol has received attention as a low-emission alternative fuel to gasoline. Ethanol emits fewer hydrocarbons than gasoline, and these hydrocarbons are less reactive photochemically. Ethanol does have some serious disadvantages. It has a lower heating value (on a volume basis) and lower volatility than gasoline. This results in poorer fuel economy and cold-startability than gasoline. One way to overcome this problem is to catalytically decompose ethanol into hydrogen, carbon monoxide, and methane on-board the vehicle. The decomposition products have a higher energy content than ethanol, and are easily combusted in cold weather. However, ethanol decomposition is an endothermic reaction. Thus it does not lend itself to direct cold-start applications. Direct cold-start implies that the catalytic converter system generates the cold-start agents (CO, CH_4 and H_2) at ambient temperature. During cold-start, the catalytic converter would have to be heated to the desired reaction temperature and then additional heat would be required to overcome the reaction endotherm. As the ambient temperature decreases, the battery power requirements increase and at some point there is insufficient power to operate both the reactor and engine starter motor.

Very little work has been conducted on the ethanol decomposition reaction. There is a need to understand the fundamental chemistry of the

surface reaction and there is also a need for highly active, highly selective, and thermally stable catalysts. Catalysts which are known to decompose ethanol include metals, metal oxides, and supported metals. The goal of most studies is to increase the selectivity of the catalysts; namely, to reduce the formation of by-products such as ethylene, and to maintain the catalyst activity.

Chanter 1
LITERATURE REVIEW

Studies of the ethanol decomposition process have used a variety of test apparatus and catalysts. The catalysts reported in the literature can be categorized into three groups: metal single crystals, metal oxides or supports, and supported metals. However, only a few studies of the reaction have used supported metal catalysts.

1.1 Ethanol Reaction on Metal Single Crystals

Mechanisms of ethanol decomposition were proposed on Pd(111) and Ni(111), which are in group VIIIB. These are helpful in determining the mechanism on supported palladium and platinum catalysts.

1.1.1 Mechanism of Ethanol Decomposition on Pd(111)

The mechanism of ethanol decomposition on Pd(111) single crystal metal catalyst has been studied by Davis and coworkers (*Davis, 1987, 1990*) using high resolution electron energy loss spectroscopy (HREELS) and temperature programmed desorption (TPD) under a standard ultra-high vacuum ($1x10^{-10}$

Torr). They revealed that the reaction proceeds through a decarbonylation pathway. The reaction is initiated by dissociative adsorption of ethanol to adsorbed ethoxy species and hydrogen. The mechanism is demonstrated in ***Figure 1***. The adsorbed ethoxy species, which is relatively unstable on the clean Pd(111) surface, then decomposes below -73°C to acetaldehyde and a surface acetyl species. Finally, at temperatures above 7°C the acetyl species decomposes to carbon monoxide, hydrogen, and methane. Acetaldehyde desorption was not observed in TPD experiments. This indicates that it is only a surface intermediate. Methane is formed from hydrogenation of surface methyl. The temperature at which methane is detected is about 73°C. A small amount of surface carbon was observed. Davis suggested that it was from the decomposition of the surface methyl which competed with the hydrogenation.

1.1.2 Mechanism of Ethanol Decomposition on Ni(111)

The reaction on a Ni(111) single metal crystal catalyst has been studied by using scanning kinetic spectroscopy (SKS), temperature programmed desorption (TPD), and Auger electron spectroscopy (AES) (*Gates, 1986*). The proposed sequence of bond breaking is shown in ***Figure 2***. The first step is the breaking of the O-H bond to form an adsorbed ethoxy and hydrogen. The second step is dehydrogenation of the methylene group ($-CH_2-$), followed by the carbon-carbon bond breaking, and dehydrogenation of the methyl group ($-CH_3$). The mechanism proposed is illustrated in ***Figure 3***. The products observed were acetaldehyde, methane, hydrogen, carbon monoxide, and surface carbon whose formation is similar to that on Pd(111).

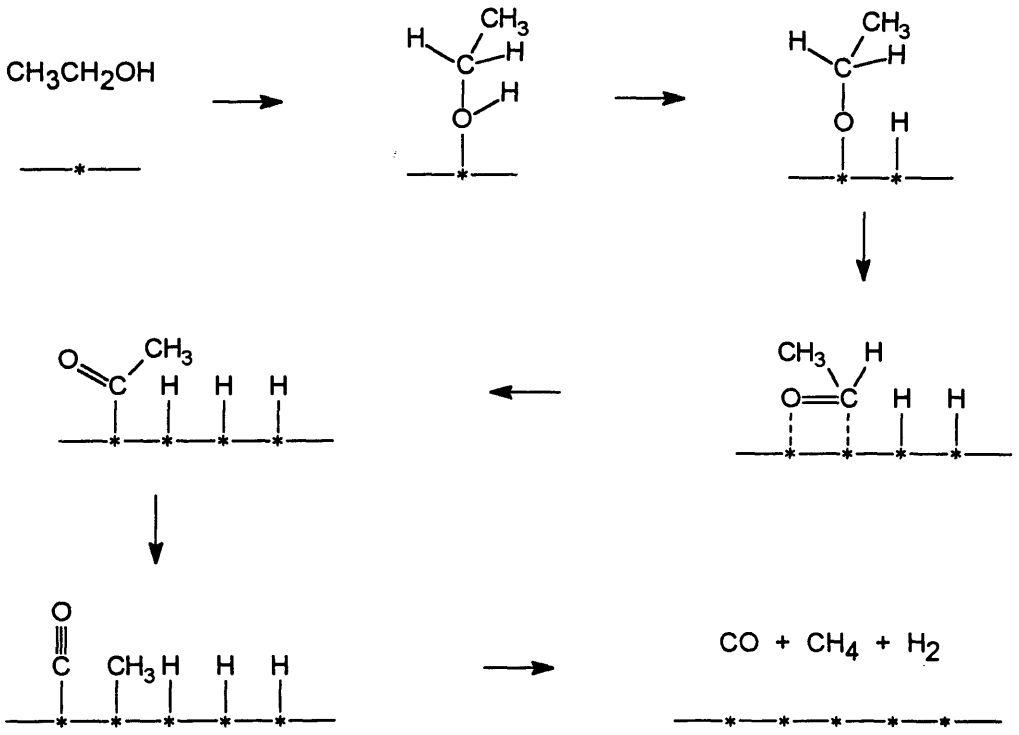

Figure 1. Mechanism of ethanol decomposition over Pd(111) (Davis et al., 1987).

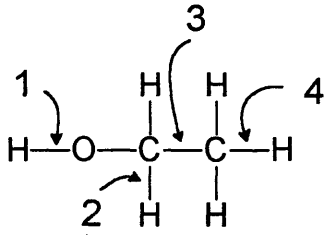

Figure 2. The sequence of ethanol bond breaking on Ni(111) (Gates et al., 1986).

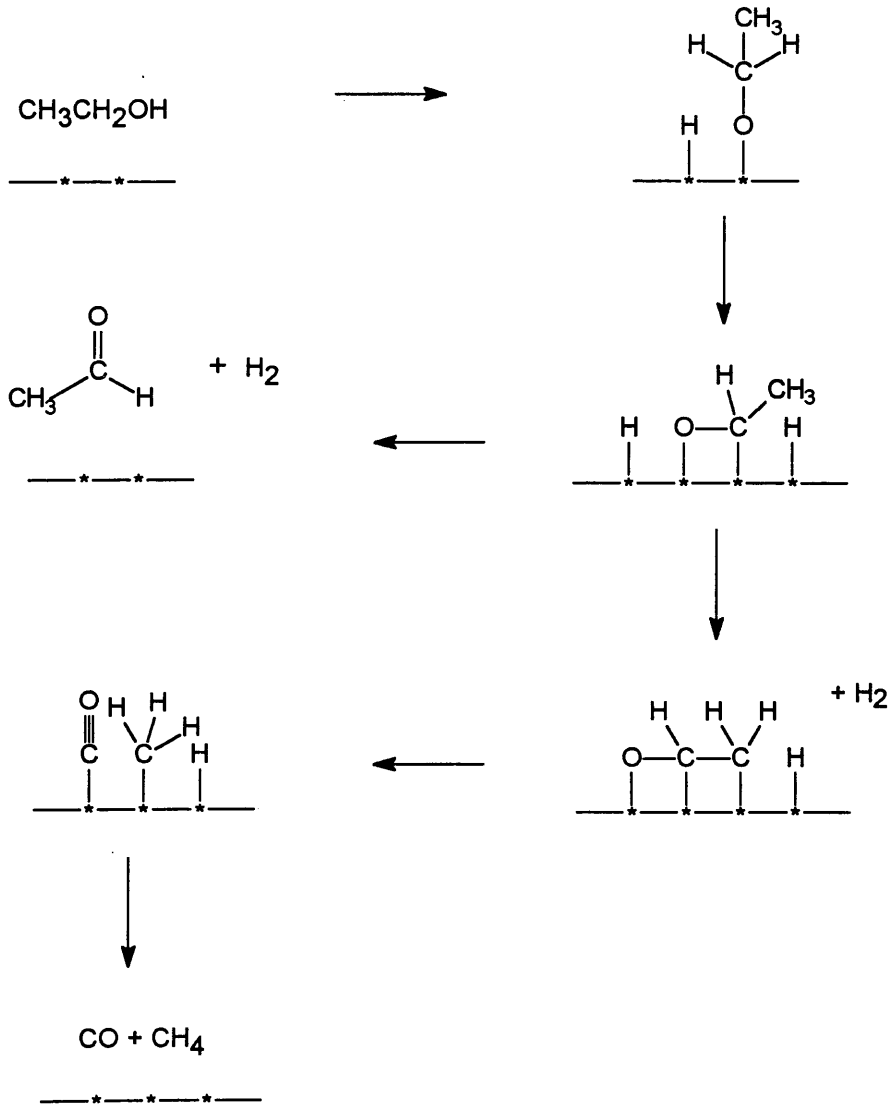

Figure 3. Mechanism of ethanol decomposition over Ni(111) (Gates et al.,1986).

The previous mechanism was confirmed by Xu and coworkers by using infrared absorption spectroscopy (IRAS), x-ray photoelectron spectroscopy (XPS), and TPD methods (*Xu, 1991*). They reported that ethanol decomposition on Ni(111) originated with O-H bond cleavage of adsorbed ethanol to form an ethoxy group in the temperature range between -108 and -73°C. This occurs while the O-H bond is almost parallel to the surface and causes the O-H stretching mode in IRAS spectra to disappear during the dissociative adsorption. In addition, during the decomposition of ethanol to the surface ethoxy group, the methyl group in the ethoxy species orients itself to have a C-H bond nearly parallel to the Ni (111) surface before cleavage to form acetaldehyde. Then C-C bond breaking occurs. In the presence of hydrogen, methane is formed and desorbed. However, this reaction competes with the decomposition of methane to form surface carbon which decreases surface activity. The formation of diethyl ether and ethylene were not reported.

1.2 Ethanol Reaction on Metal Oxide Supports

Two metal oxide supports are discussed in this section, Al_2O_3 (alumina) and SiO_2 (silica). These two supports have been widely used as catalytic supports due to high mechanical strength, thermal stability, and high surface area. Active sites and reactivity on both supports are discussed.

1.2.1 Ethanol Reaction on Alumina

Hydrated alumina is activated by calcining at 500°C. Activated alumina is amphoteric, containing both acidic and basic sites as illustrated in ***Figure 4***

(*Diddams, 1992*). These sites are active for the dissociative adsorption of ethanol. By using infrared spectroscopy to study ethanol decomposition on alumina, it was reported that in the temperature range of 120 - 180 °C, ethanol dissociatively adsorbs as ethoxy groups and surface hydrogen (*Soma, 1968*). Then the surface ethoxy reacts through one of the two pathways as shown in ***figure 5***. The first pathway, which occurs above 220°C, involves the formation of diethyl ether and water from two ethoxy groups, since the adsorbed species can migrate all over the surface. This is substantiated by the fact that diethyl ether dissociatively adsorbs as surface ethoxy groups. Above 180°C, the reaction products were only ethylene and water from the reaction between the adsorbed ethoxy species and surface hydroxy. The overall process is referred to as ethanol dehydration. The rate of decomposition is independent of ethanol pressure; i.e., it is zero order in ethanol.

1.2.2 Ethanol Reaction on Silica

The surface of amorphous silica consists of siloxane (Si-O-Si) and silanol (Si-OH) groups (*Diddams, 1992*). In ***Figure 6***, silanol groups are identified as a weak Bronsted acids. From the study of hydrogen bonding of alcohol on silica *(Metcalfe, 1977*), alcohols such as ethanol can adsorb by two different pathways as illustrated in ***Figure 7***. An esterification of surface hydroxyl groups occurs at higher temperature while a surface alkylation taking place through opening of strained siloxane bonds occurs at lower temperature and may be completed at room temperature (*Jeziorowski, 1973*).

On porous Vycor silica glass, the reaction of ethanol was studied by using infrared spectroscopy at room temperature. The observed reaction was ethanol

dehydration which proceeded through surface alkylation. This was the route of ethylene formation at the surface. In addition, when the glass surface was treated with Na^+ ions in order to incapacitate Bronsted acid centers by exchanging with the replaceable proton, the ethylene formation was suppressed (*Metcalfe,1977*).

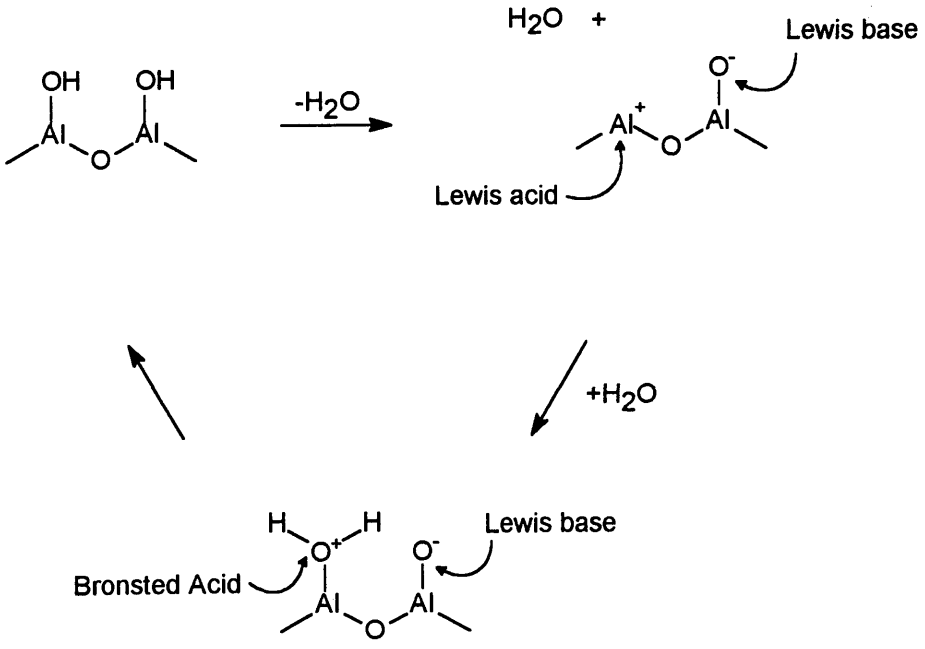

Figure 4. Basic and acidic sites on alumina (Diddams, 1992).

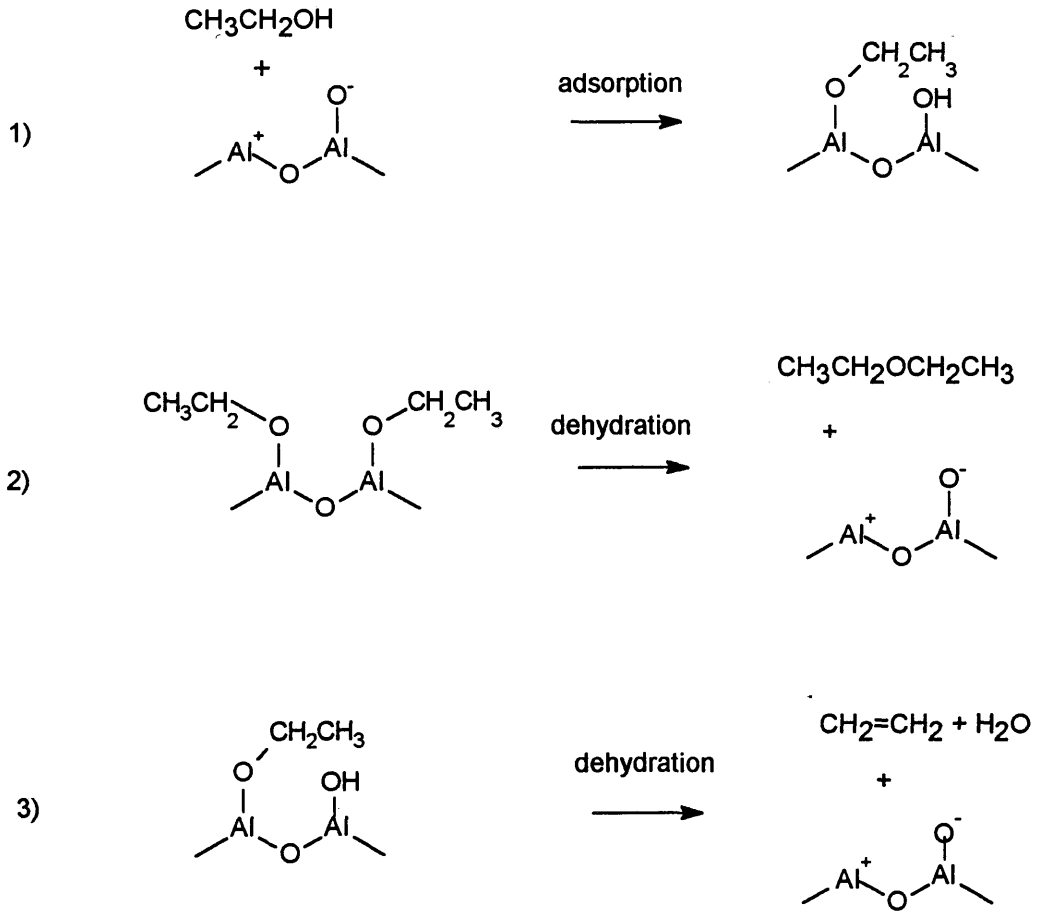

Figure 5. Ethanol reactions on alumina.

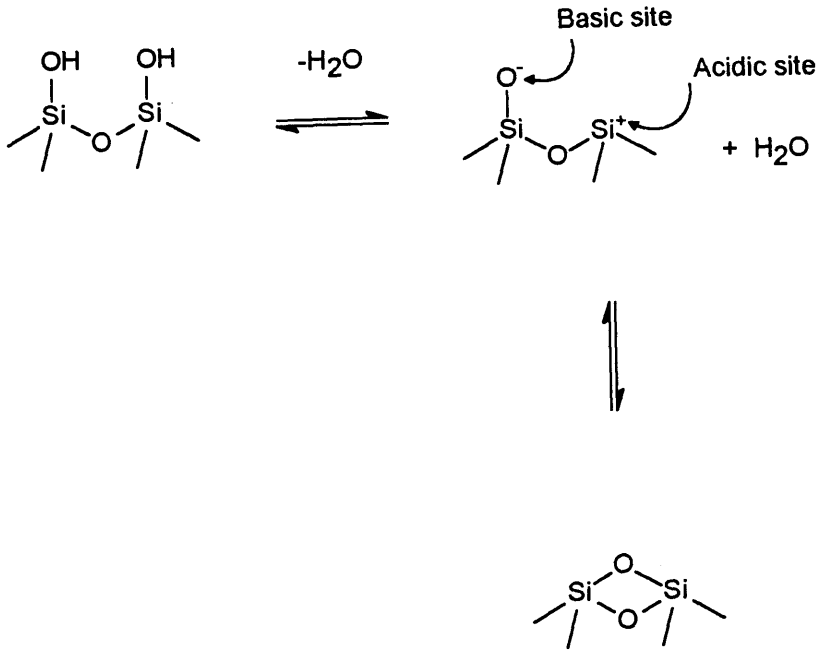

Figure 6. Basic and acidic sites on silica.

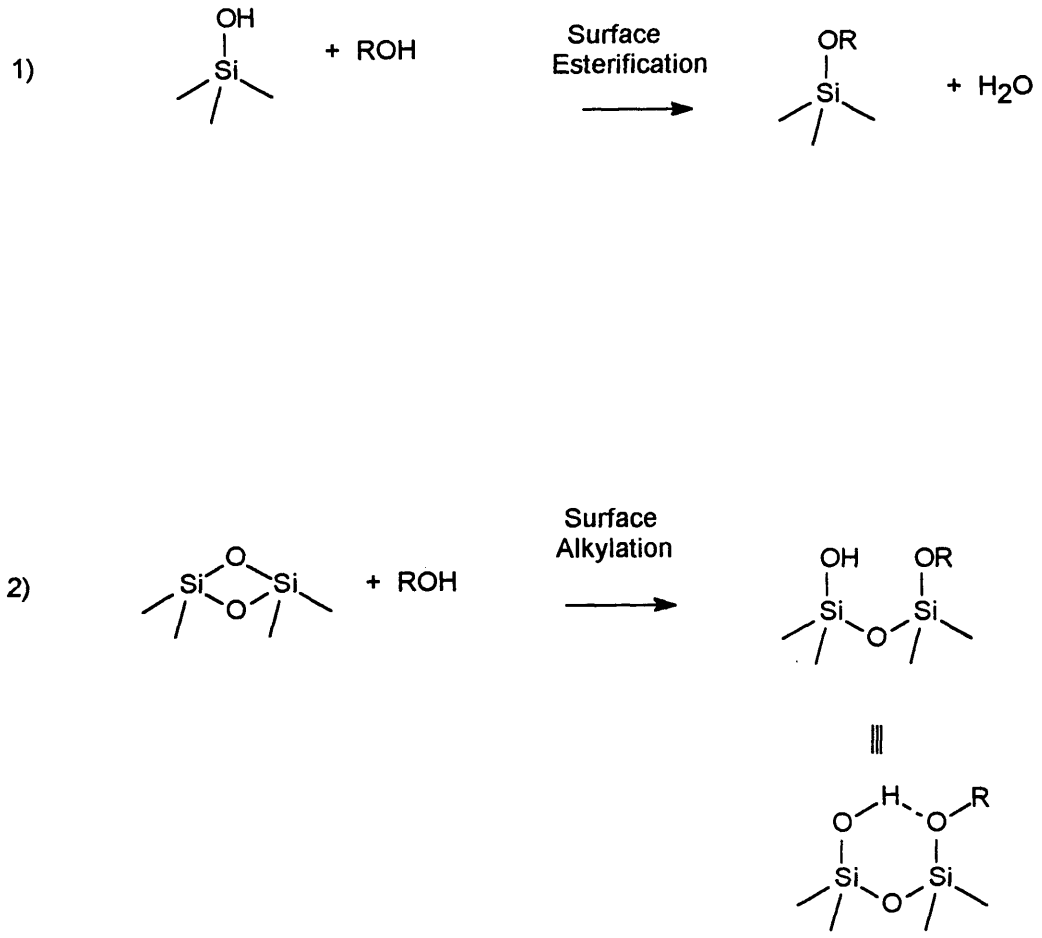

Figure 7. Alcohol adsorption on silica (Jezioroski et al., 1973).

1.3 Ethanol Reaction on Supported Metal

The ethanol decomposition discussed below was studied on two catalysts, zinc oxide-supported palladium and alumina-supported palladium.

1.3.1 Ethanol Reaction on Zinc Oxide-Supported Palladium (Pd/ZnO)

On Pd/ZnO, ethanol decomposition was observed through two reaction pathways: dehydrogenation to acetaldehyde and hydrogen (equation (1.1), and dehydration to ethylene and water (equation 1.2) (*Mokwa, 1983*).

$$CH_3CH_2OH \rightarrow CH_3CHO + H_2 \quad (1.1)$$

$$CH_3CH_2OH \rightarrow C_2H_4 + H_2O \quad (1.2)$$

$$CH_3CHO \rightarrow CO + CH_4 \quad (1.3)$$

These reactions were similar to that observed on the ZnO surface (*Mokwa, 1982*). At a higher coverage of Pd, acetaldehyde decomposes to carbon monoxide and methane as shown in equation (1.3). This reaction was dominant over reaction (1.1) and (1.2).

1.3.2 Ethanol Reaction on Alumina-Supported Palladium (Pd/Al_2O_3)

For palladium on alumina, the reaction was conducted as steady-state flow experiments in a Berty reactor at 180-230°C. This temperature range was selected because the dehydration of ethanol on alumina was negligible below 230°C. It was reported that ethanol decomposition was a two-step reaction

(*Davidson, 1989*). The first step is ethanol dehydrogenation to acetaldehyde and hydrogen (equation 1.1) and the second step is acetaldehyde decomposition (equation 1.3) . The main products are hydrogen, methane, and carbon monoxide with a trace of acetaldehyde, ethylene, diethyl ether and carbon dioxide. Carbon dioxide was attributed to the reaction between carbon monoxide and water (equation 1.4). This reaction is referred to as the water-gas shift or stream-reforming reaction.

$$CO + H_2O \rightarrow CO_2 + H_2 \qquad (1.4)$$

Metals which are able to catalyze aldehyde decarbonylation effectively are platinum (Pt), ruthenium (Ru), nickel (Ni), Tungsten (W), and palladium (Pd). These metals have high CO and H_2 chemisorption heats. Comparing alumina-supported Ru, Rh, Pd, and Pt catalysts, Pd demonstrates the highest yield of methane per gram of metal. In addition, alumina-supported Pd also catalyzed acetaldehyde hydrogenation to ethanol, and thus the reverse reaction is possible.

Davidson and coworkers also observed that the yield of methane production is lower in the presence of hydrogen, carbon monoxide, and water. It indicates that the above reactions are inhibited by hydrogen, carbon monoxide, methane and water. Hydrogen can retard the reaction because its adsorption prevents the dissociative adsorption of ethanol to form surface ethoxy groups and hydrogen. The inhibiting role of methane in the reaction is still obscure. It was suggested that methane retards the chemisorption of acetaldehyde which has been thought to be an intermediate in the ethanol decomposition process.

According to the above review ethanol decomposition on single crystal metals has been successfully studied over Pd(111) and Ni(111) and reasonable mechanisms on these catalysts have been proposed. However, those were done under an ultra-high vacuum which is not practical in industry. To decrease energy consumption and increase practicability, the reaction was conducted at atmospheric pressure. Metals used were palladium and platinum, which are in group VIIIB. To increase the metal surface area, palladium and platinum were deposited on a solid support. Silica was considered the best candidate for a solid support because it is thermally stable, porous, and inert.(*Diddams, 1992*) However, it contains acidic sites which promote the dehydration. In order to reduce the support acidity, the support was coated with a basic material. Lanthanum oxide (La_2O_3 or lanthana) has been reported as a good candidate (*Castiglioni, 1992* and *Wickham, 1986*). The surface basicity of lanthana-silica increases with the lanthana loading. At 75-percent weight lanthana loading, the basicity of the support is similar to that of pure lanthana. It was also reported that lanthana increases the activity of silica towards the oxidation and hydrogenation of carbon monoxide. However, there has been no report about using metal deposited on lanthana-modified supports in ethanol decomposition. The effect of lanthana on catalyst properties, such as activity and stability, as well as the reaction mechanisms were studied.

Chapter 2
STATEMENT OF PROBLEM

There are four problems that were addressed in this study.

1. Thermodynamic calculations were conducted to estimate the feasibility of the decomposition and dehydration of ethanol over a temperature range of 200 to 500°C, and of other possible reactions that might have been encountered in this study. The results were compared to catalyst testing results to consider whether or not the studied reactions approach the thermodynamic equilibrium.

2. This experimental study attempted to find the best conditions for a high yield of hydrogen, carbon monoxide and methane from ethanol. The conditions which were considered were the temperature, catalyst contact time, and particle size.

3. It is important to design and test a catalyst with high activity and selectivity for the decomposition reaction. Effective supported catalysts have not yet been developed. A satisfactory catalyst must provide good metal dispersion, low surface acidity, high surface area, and good mechanical strength.

4. There is a need to better understand the fundamental mechanism of the surface decomposition of ethanol, which is the desired reaction, as well as, to understand the undesired reaction, ethanol dehydration.

Chapter 3
EXPERIMENTAL PROCEDURE

3.1 Chemicals and Materials

The chemicals used for this study can be divided into four categories: cylinder gases, reactants and calibration liquids, catalyst preparation materials, and XRD calibration standards. All chemicals were used as received without further purification.

3.1.1 Cylinder gases

The cylinder gases consisting of high purity grade helium (99.995%), ultra high purity grade hydrogen (99.999%), 2.0% hydrogen in helium, and a multicomponent calibration gas, were obtained from General Air Service and Supply Company (Denver, CO). The high purity helium was used as a purge gas and a diluent gas in the catalytic reactor system. The ultra high purity hydrogen was used to reduce the catalyst to the active metal form. The 2.0% hydrogen/98.0% helium mixture was used as a carrier gas for the gas chromatograph. The multicomponent calibration gas which contained 0.49 % ethane, 4.96 % ethylene, 0.50 % acetylene, 14.97 % methane, 14.98 % carbon

dioxide, 38.33 % carbon monoxide and 25.86 % hydrogen by volume and was used to calibrate the gas chromatograph.

Standard CP grade ethane, carbon monoxide, and methane were obtained from Scientific Gas Products, and standard CP grade ethylene was obtained from the Linde Division of Union Carbide Corporation. These gases were used to verify the retention times of the gaseous reaction products observed in this study.

3.1.2 Reactants and Calibration Liquids

The ethanol (100%) and acetaldehyde (90-95%) reactants used in this study were supplied by McCormic Distilling Company, Incorporated, and Mallinckrodt, Incorporated, respectively. Known alliquotes of these liquids were mixed with water to produce a liquid calibration standard for the gas chromatograph.

3.1.3 Catalyst Preparation Materials

The grade 57 silica gel used as the catalyst support was supplied by Davison Chemical. An analysis of the silica material, provided by Davison Chemical, showed it to be composed of 99.5% SiO_2, 0.05% Al_2O_3, 0.1% Na_2O, 0.05% sulfate, 0.03% iron, 0.10% CaO, and >0.01% chloride. The total surface area is 300 m^2/g and the pore volume is 1.0 cc/g. The lanthanum nitrate hydrate (99.999% with maximum 0.001% Ca) was obtained from Fisher Scientific Company. The palladium (II) chloride (59.75%Pd) and platinum(IV) chloride were supplied by Strem Chemicals, Incorporated. The concentrated

hydrochloric acid used to prepare palladium salt solution was supplied by Mallinckrodt, Inc.

3.1.4 XRD Calibration Standards

Palladium powder and platinum screen supplied by Alfa Products, Thiokol/Ventron Division were used as XRD calibration standards.

3.2 Catalyst Preparation

The catalysts were prepared using standard impregnation methods.(*Logsdon, 1989* and *Wickham, 1986*)

3.2.1 Lanthana-Doped Silica

The doped supports for the palladium and platinum catalysts were prepared according to the following procedure:

1. The primary catalyst support was obtained by grinding Grade 57 silica gel (SiO_2) granules in a mortar and pestle and collecting particles in the 14-20 mesh range.
2. The silica support particles were calcined at 550°C overnight in a Type 1300 Thermolyne muffle furnace to eliminate the adsorbed water. The temperature of the furnace was gradually increased from ambient temperature to 550°C over a 5 hour period. The calcined particles were removed from the oven, cooled to room temperature and stored in a desiccator which contained no

desiccant.

3. The wetability (or water capacity) of the support was determined by adding deionized water to a 1.0 gram sample of silica. The addition was done under a mild vacuum (~ 13-20 mm Hg) to improve the degree of pore filling by the liquid. Water was added until the particles began to visibly stick together. The wetability was 1.2 cc/g of silica.
4. A lanthanum nitrate solution was applied to the dried silica support using standard catalyst impregnation methods (*Page, 1987*). The lanthanum nitrate solution was added drop wise to a three-necked round bottomed flask containing the dried silica support with shaking. Sufficient lanthanum nitrate solution was added to obtain the desired lanthanum oxide loading. An example of the preparation is described as follows: lanthanum nitrate hydrate 0.73 g was added to 12.5 ml of deionized water. The entire lanthanum nitrate solution was slowly added to 6.56 g of silica support. This recipe produces a 5.0% weight percent loading of La_2O_3 on the SiO_2 substrate.
4. The lanthanum nitrate impregnated silica support was dried under flowing air overnight at 120°C.
5. The dried impregnated silica was calcined at 550°C overnight in a muffle furnace to decompose the lanthanum nitrate salt into lanthana (La_2O_3) and to firmly fix it to the silica surface. The support was then cooled to ambient temperature and stored in a desiccator. The lanthana modified silica (La_2O_3/SiO_2) was used as a support material for the platinum and palladium catalysts. The

modified silica supports were designated as 2%La_2O_3/SiO_2 and 5%La_2O_3/SiO_2 in which 2.0 and 5.0 weight percent loading of lanthanum oxide was fixed to the silica surface.

3.2.2 Palladium-Based Catalyst

For palladium-based catalysts, the supports were silica and lanthanum-modified silica. The preparation procedures were as follows:

1. The previously calcined SiO_2 and La_2O_3/SiO_2 support was impregnated with a solution of palladium by an incipient wetness technique. The solution used was prepared by dissolving palladium(II) chloride in a 1:1 by volume mixture of water and concentrated hydrochloric acid. In this preparation, the solution was heated at about 80°C for 30 minutes to promote dissolution of the palladium salt. Using the water capacity measurement obtained previously for the silica particles, a sufficient amount of the palladium salt was added to obtain a two weight percent loading of palladium metal on the finished catalyst.
2. After impregnation, the catalyst was dried overnight under flowing air at 120°C.
3. The dried catalyst was calcined overnight at 550°C in a muffle furnace to decompose the palladium salt into small palladium metal or metal oxide crystallites. Then the catalyst was cooled down and stored in a desiccator. The catalysts prepared were designated as 2%Pd/2%La_2O_3/SiO_2 , 2%Pd/5%La_2O_3/SiO_2 and 2%Pd/SiO_2.

3.2.3 Platinum-Based Catalysts

The preparation procedures of platinum-based catalysts were similar to those of palladium catalysts. The solution was prepared by dissolving platinum(IV) chloride in water and repeating the procedure steps used for preparation of the palladium catalysts. Again, the supports were SiO_2 and La_2O_3/SiO_2. The catalysts prepared were designated as $2\%Pt/2\%La_2O_3/SiO_2$, $2\%Pt/5\%La_2O_3/SiO_2$ and $2\%Pt/SiO_2$.

4.3 Catalyst Characterization

Two techniques were used for catalyst characterization: X-ray powder diffraction(XRD) and X-ray photoelectron spectroscopy (XPS). The first technique was used for all freshly calcined and tested catalysts while the second technique, conducted by the Physical Electronics Laboratories in Minnesota, was used for only the freshly calcined $2\%Pt/SiO_2$ and $2\%Pt/5\%La_2O_3/SiO_2$.

4.3.1 X-ray Powder Diffraction (XRD)

Both freshly calcined and the final tested catalysts were characterized by the XRD technique. This was done to determine whether or not the metal or metal oxide form of platinum or palladium was present on the calcined and tested catalysts. In addition, XRD line broadening methods were employed to determine the degree of dispersion of palladium, platinum, and/or lanthana component on the silica surface. The XRD line patterns for the catalysts were compared to reference silica, lanthana, palladium powder and a metal gauze

sample of platinum.

To prepare XRD samples, each catalyst was ground to a fine powder (< 200 mesh) using a mortar and pestle, and placed in a conventional aluminum sample holder. The XRD patterns for the catalyst and reference samples were obtained using a Rigaku XRD instrument. The x-ray was generated from a copper K_α target using a current of 55 mA and a potential of 60 kV. The scans were performed between 2θ values of 10 and 100 degrees at a scan rate of 5 degrees per minute. The signal intensity versus reflection angle were recorded.

The dispersion of palladium, platinum or lanthana on silica support material was determined using line broadening techniques. During the calcining step, the palladium, platinum and lanthanum salt decompose into a highly dispersed oxide layer on the silica or coalesce into small metal or metal oxide crystallites. When the average crystallite diameter is less than 1000 A° a factor, called pure diffraction broadening (β), contributes to the total breadth *(b)* and causes line broadening beyond that expected from the instrument. Pure diffraction broadening increases with decreasing crystallite size, and the lines become so broad and finally indistinguishable from the background (*Nuffield, 1966.*) The mean metal crystallite diameter (*D*), in A°, can be calculated from the following equation:

$$D = \frac{k\,\lambda}{\beta\,\cos\theta}$$

where

$$\beta = \sqrt{B^2 - b^2}$$

where k = shape factor, related to crystallite shape (taken as 0.9) (*Cullity, 1978*)

λ = X-ray wavelength, for Cu K_α = 1.5418 A°

θ = diffraction angle

β = Pure breadth of a powder diffraction

B = Breadth at half the maximum intensity of sample

b = Breadth at half the maximum intensity of metal standard

In addition, the availability of metal can be estimated, assuming the crystal is cubic, by the following formula (*White, 1989*):

$$\text{surface area/g metal} = 5/d\rho$$

where d = crystallite diameter

ρ = metal density

3.3.2 X-ray Photoelectron Spectroscopy (XPS)

In x-ray photoelectron spectroscopy, a sample is bombarded with monochromatic photons, such as Al Kα, which eject electrons from core and valence shells in which the ionization potential, or binding energy, is less than the primary photon energy. The kinetic energy of the ejected electrons is measured and is related to the binding energy as follows:

Photon Energy = Binding Energy + Kinetic Energy.

The element from which the electron was ejected can be identified by comparing the measured binding energy with tables of x-ray absorption data.

3.4 Catalyst Pretreatment

Before catalyst evaluation, the catalysts were reduced by the following procedure:

1. Approximately 0.400 grams of catalyst (14-20 mesh) were mixed with 1.000 gram of quartz chips (10-14 mesh) and loaded into the quartz reactor tube. The catalyst bed was supported by a coarse fritted quartz disk which had been fused to the quartz tube. The catalyst bed was positioned in the isothermal zone of the oven. The quartz chips were used to improve the flow characteristics through the catalyst bed and to minimize heat transfer problems.
2. After the reactor system was purged with helium (20 ml/min) for 30 minutes, a hydrogen flow (20 ml/min) was introduced. The system was tested for leaks using a TIF 8800 flammable gas detector.
3. The reactor was heated at a rate of 10°C/min to 400°C and held at this temperature for 2 hours.
4. The system was purged with helium (20 cc/min) and the catalyst bed was cooled to the room temperature.
5. At this point, The computerized catalyst heating sequence was initialized.

3.5 Catalytic Reactor System

Catalyst evaluations were conducted in a tubular flow reactor by the scheme shown in ***Figure 8***. Ethanol was loaded into a 10 cc gas tight syringe and introduced into the preheater via a Model 341A Sage syringe pump with the rate of 1.5 cc/hr. An 18-inch needle attached to the syringe was inserted through a septum into the base of the preheater. The preheater was maintained at 110°C to insure vaporization of ethanol. The vaporized ethanol was mixed with helium gas flow (20 cc/min) before entering the catalytic reactor tube. The ethanol pump rate of 1.5 cc/min and helium gas flow of 20 cc/min produced a space velocity of 3.5 hr^{-1}. The reactor tube was heated in a Type 54031 Lindberg furnace in which the heating sequence was controlled by an EG Control automated system. The catalytic testing sequence began by heating the reactor from ambient temperature at a rate of 10°C/min to 200, 300, 400, and 500°C. The temperature was held for three hours at each temperature. Finally, the reactor was cooled to 300°C to observe loss in catalytic activity. The catalyst bed temperature was monitored by a type-K thermocouple.

The reaction products from the quartz reactor tube passed through a heated (100°C) exit line to prevent condensation. The product stream was sampled and analyzed by an on-line gas chromatograph and the remainder was vented into the hood.

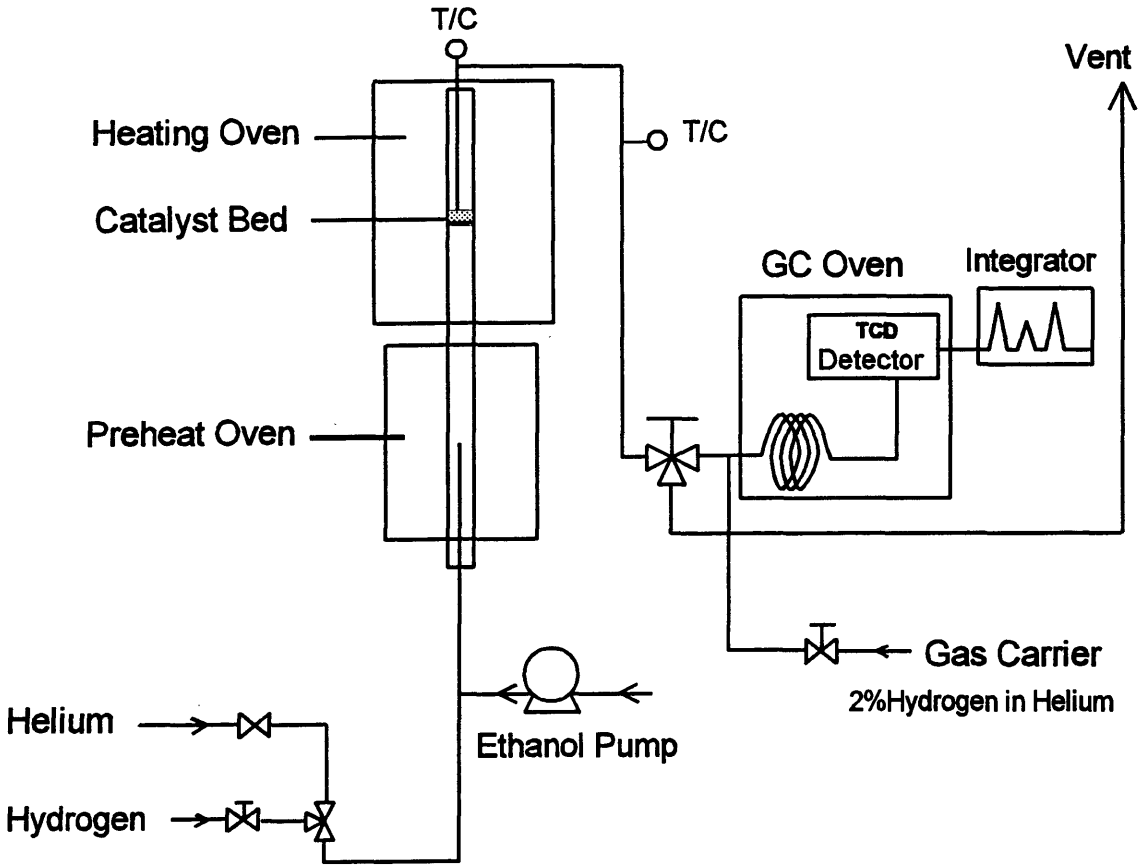

Figure 8. The reactor system used to evaluate catalyst materials.

3.6 Gas Chromatograph

The products were analyzed by a Perkin-Elmer Sigma-3B gas chromatograph (GC) with a thermal conductivity detector (TCD). A carrier gas consisting of approximately 2.0 mole % hydrogen in helium was used. This carrier gas mixture is required when hydrogen analysis is desired. The carrier gas flow rate was 30 cc/min. The analytical column was a 10' x 1/8" stainless steel tube packed with porapak N (80-100 mesh). The analysis was performed using an initial oven temperature of 80°C, increasing temperature at a rate of 20°C/min to 150°C, and finally holding at that temperature for 15 minutes. The injector temperature was 125°C and the TCD detector temperature was 235°C. The GC was calibrated using a certified gas mixture containing ethane, ethylene, acetylene, methane, carbon dioxide, carbon monoxide and hydrogen, and a liquid mixture containing ethanol, water and acetaldehyde. These were components observed in the product stream. The weight response factors of the compounds were determined from mole percents and peak areas according to the method given in ***Appendix 2*** (*Perry, 1981*).

Chapter 4
RESULTS OF THERMODYNAMIC CALCULATIONS

Thermodynamic data can provide two important pieces of information needed in this study, the heat of reaction (ΔH_r °) and the Gibbs free energy of reaction (ΔG_r°). Thermodynamic analysis also allows the calculation of the equilibrium constant (K_p) from ΔG_r ° . With the equilibrium constant known, the equilibrium product yield for a given set of reactions can be estimated.

The objective of this work was to determine the ΔG_r ° values for all the potential surface reactions that may occur during the catalytic decomposition of ethanol over a temperature range of 100 - 1000 °C. This information was used to determine the feasibility of a given reaction and to predict the expected equilibrium distribution of reactants and products. The thermodynamic feasibility of a reaction is defined by the criteria shown in ***Table 1***. According to Richardson, reactions with a ΔG_r ° value of +10 kcal/mole and greater are not feasible for most applications. Reactions with a ΔG_r ° value of zero to 10 kcal/mole are only feasible under special reaction conditions, and of course reactions with a ΔG_r ° value less than zero are considered most useful. Since the reactions are to be conducted on board a vehicle, it is important that the reaction of interest be as spontaneous as possible.

Table 1 The criteria for thermodynamic feasibility *(Richardson, 1989)*

ΔG_r °	Feasibility
1. Very negative, < -10 kcal/mole	Very high equilibrium conversion possible
2. Moderately negative, 0 to -10 kcal/mole	Fairly high equilibrium conversion possible
3. Moderately positive, 0 to 10 kcal/mole	Low equilibrium conversion depending upon process conditions
4. Very positive, > 10 kcal/mole	very low equilibrium conversion, generally not significant reactions

The ΔG_r ° and ΔH_r ° values for the various reactions were calculated using a program developed at the Colorado School of Mines (CSM) by this author. The results were compared to those obtained from two commercial software packages, CHETAH (7.0) and ASPEN PLUS. The ΔG_r° values obtained for the three programs are in excellent agreement with a variance less than 0.1 for the reactions (4.1), (4.4), and (4.5), thus, giving a high degree of confidence in the data.

Details of calculation method, the property data bank, and the computer program for the CSM software are given in ***Appendix 1***. The reactions considered for this study are ethanol decomposition (equation 4.1), ethanol dehydrogenation (equation 4.2), acetaldehyde decomposition (equation 4.3),

$$CH_3CH_2OH \rightarrow CO + CH_4 + H_2 \quad (4.1)$$

$$CH_3CH_2OH \rightarrow CH_3CHO + H_2 \quad (4.2)$$

$$CH_3CHO \rightarrow CH_4 + CO \quad (4.3)$$

$$CH_3CH_2OH \rightarrow CH_2{=}CH_2 + H_2O \quad (4.4)$$

$$2\ CH_3CH_2OH \rightarrow CH_3CH_2OCH_2CH_3 + H_2O \quad (4.5)$$

and ethanol dehydration (equations 4.4 and 4.5). Based on work reported in the literature and work conducted on this project, the overall ethanol decomposition reaction (equation 4.1) can be viewed as a two-step process involving ethanol dehydrogenation (equation 4.2) followed by acetaldehyde decomposition (equation 4.3).

For cold-start applications, ethanol decomposition is an acceptable reaction because it generates combustible gaseous products which would assist the combustion process, see equation (4.1). Ethanol dehydration (equation 4.4) to form diethyl ether is also an acceptable side reaction, since diethyl ether is a known cold-start agent. However, conditions that support ether formation may also support ethylene formation (equation 4.5). Ethylene in the product stream can cause rapid deactivation (coking) of the catalyst, especially at low partial pressures of hydrogen. The focus of this work is to determine the feasibility of the ethanol decomposition reaction for cold-start applications.

The ΔG_r ° and ΔH_r ° values for reactions (4.1), (4.4) and (4.5) are plotted versus temperature and the results are shown in ***Figures 9*** and ***10***. The decomposition reaction (equation 4.1) and one of the dehydration reactions (equation 4.4) are significantly endothermic. Highly endothermic reactions

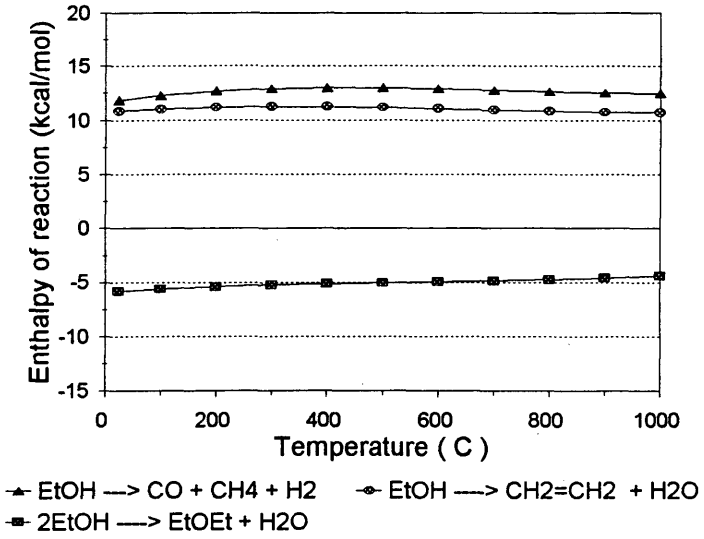

Figure 9. Enthalpy of reaction versus temperature for the ethanol decomposition and dehydration reactions.

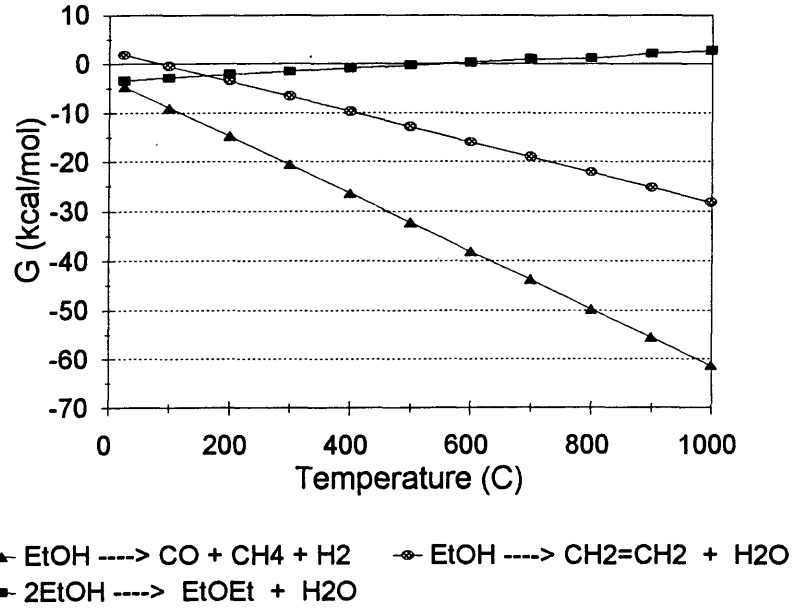

Figure 10. Gibbs free energy of reaction versus temperature for the ethanol decomposition and dehydration reactions.

do not lend themselves to direct cold-start applications. However, ethanol decomposition would work using an indirect cold-start method, where the cold-start agents are generated after the engine has reached normal operating temperatures. The agents would be stored on-board the vehicle and introduced along with ethanol for cold starting and cold operation of the vehicle.

The dehydration reaction to form diethyl ether (equation 4.5) is exothermic and may be considered as an alternative candidate for the direct cold-starting of a vehicle. Once the reaction is initiated, the reaction exotherm will reduce the power requirement needed for heating the catalytic converter. However, the selective generation of diethyl ether as opposed to ethylene may be a difficult challenge to meet.

The $\Delta G_r°$ values for the reactions (4.1), (4.4) and (4.5) are presented in ***Figure 10***. All of the reactions are thermodynamically spontaneous between 100 and 500°C, which suggests that good product yields are possible. Ethylene formation becomes non-spontaneous below 100°C. Therefore, the temperatures that favor good equilibrium yields for the ethanol decomposition and diethyl ether formation reactions, and poor yields for the ethylene production, occur below 100°C. However, at such low temperatures ethanol decomposition and diethyl ether production reactions may be kinetically limited. The rate of methanol decomposition is known to be very low at temperatures below 200°C using metal supported catalysts.(*Logsdon, 1989*) Ethanol decomposition is also expected to be kinetically limited in this temperature range.

Although the overall ethanol decomposition reaction is highly spontaneous, the reaction is thought to occur via a two-step process involving ethanol dehydrogenation (equation 4.2) and subsequent acetaldehyde decomposition (equation 4.3). If one of these steps is thermodynamically

unfavorable, then the overall process may be limited by that reaction. The $\Delta G_r°$ and log K_{eq} values for these reactions were plotted versus temperature and the results are presented in ***Figures 11*** and ***12***. Both reactions are spontaneous above 300°C. Ethanol dehydrogenation is not thermodynamically favored at temperatures below 300°C, however, the equilibrium can be forced to the right if the subsequent decomposition reaction rapidly removes the acetaldehyde product from the first reaction.

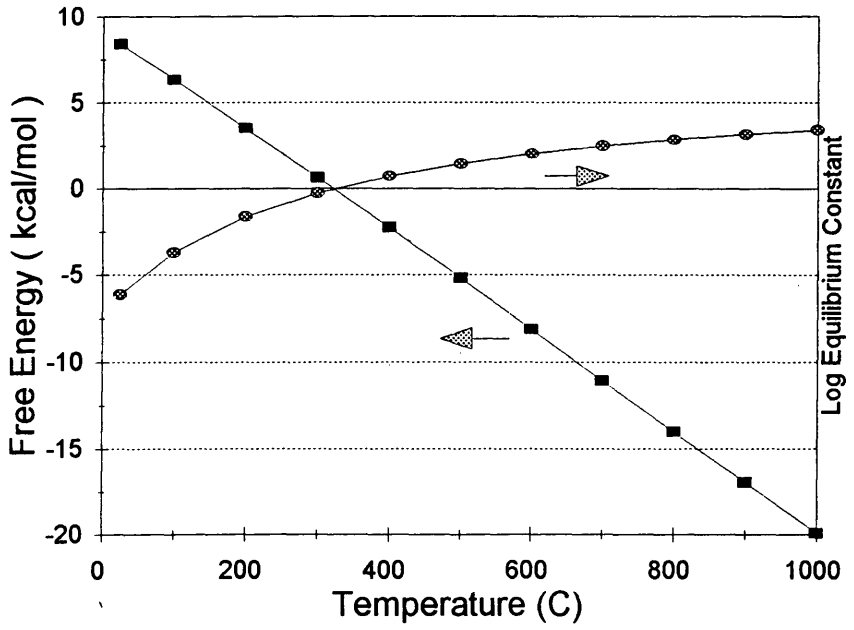

Figure 11 Gibbs free energy of reaction and log of the equilibrium constants for the ethanol dehydrogenation reaction.

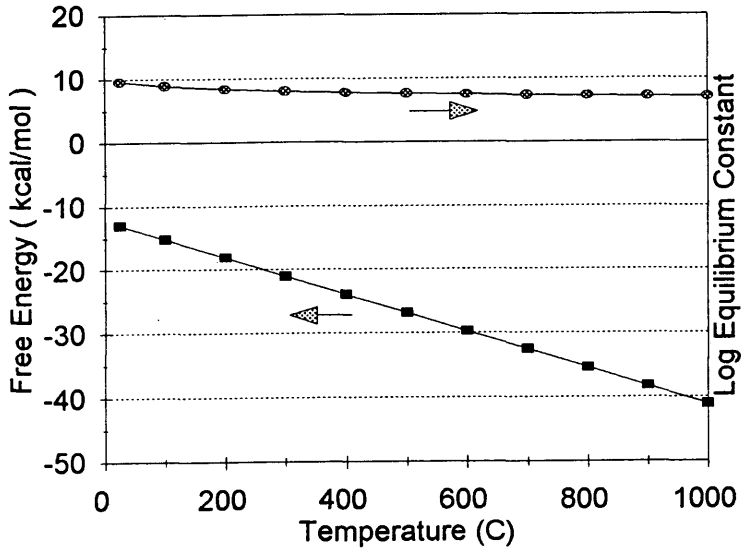

Figure 12. Gibbs free energy of reaction and log of the equilibrium constants for the acetaldehyde decomposition reaction.

In order to predict the equilibrium composition of the reactants and products, all possible side reactions must also be considered in addition to the obvious ones considered above. The additional side reactions considered are given in equations (4.6) through (4.8) below. Water may be introduced as an impurity in the ethanol feedstock or it may be generated in the catalyst bed via reactions (4.4) and (4.5). As shown in ***Figure 13***, reaction (4.6) is thermodynamically favorable throughout the temperature range. Water may react with CO, referred to as the water-gas shift reaction (equation 4.7), or it may react with methane via a steam reforming reaction (equation 4.8).

$$CH_3CH_2OH + H_2 \rightarrow CH_3CH_3 + H_2O \quad (4.6)$$

$$CO + H_2O \rightarrow CO_2 + H_2 \quad (4.7)$$

$$CH_4 + H_2O \rightarrow CO + 3H_2 \quad (4.8)$$

The $\Delta G_r°$ and log K_{eq} values for these side reactions involving water were plotted versus temperature and the results are presented in ***Figures 14*** and ***15***. The water-gas shift reaction (equation 4.7) is thermodynamically favored at temperatures below 800°C, while the methane steam reforming reaction (equation 4.8) is favored at temperatures above 600°C. Only in the narrow temperature range of 600 to 800°C do both reactions appear to be spontaneous.

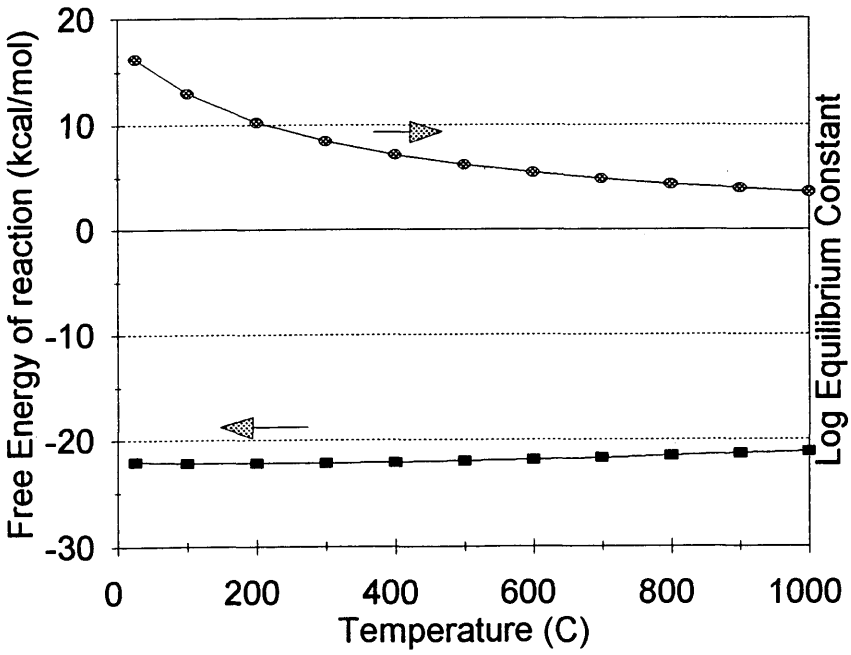

Figure 13. Gibbs free energy of reaction and log of the equilibrium constants for the reaction between ethanol and hydrogen.

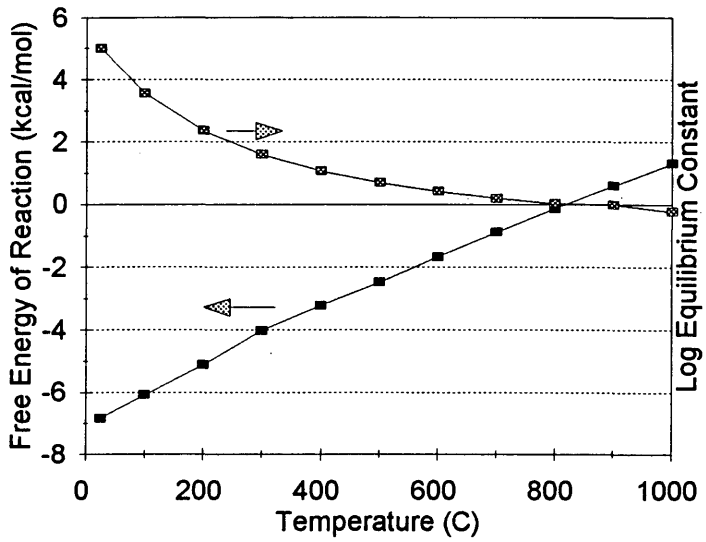

Figure 14. Gibbs free energy of reaction and log of the equilibrium constants for the water-gas shift reaction.

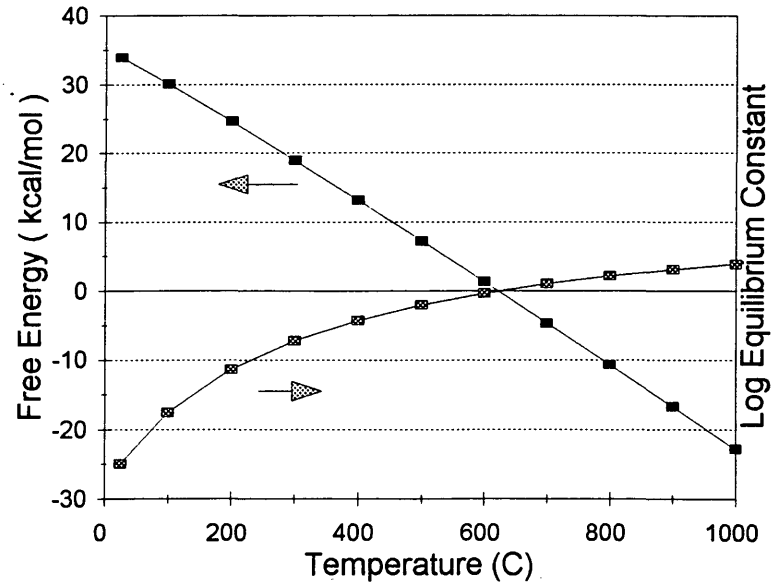

Figure 15. Gibbs free energy of reaction and log of the equilibrium constants for the methane stream reforming reaction.

The ASPEN PLUS program has the capability of determining the equilibrium mole percent of products for a system in which all of the above reactions occur simultaneously, assuming ideal gas behavior, see ***Figure 16***. If the system reaches thermodynamic equilibrium, carbon dioxide and methane are the major products between 100 and 400°C. The product distribution goes through a transition between 400 and 600°C, and finally carbon monoxide, methane and hydrogen are the major products in the 700 to 1000°C temperature range. The ASPEN PLUS results suggest that methanation (a reverse reaction of equation 4.8) and water-gas shift reactions (equation 4.7) are predominant at the lower temperatures while methane steam reforming (equation 4.8) predominates at higher temperatures. Thermodynamic calculations suggest that dimethyl ether, ethylene and water will not be present in any significant amount at equilibrium over the temperature range studied.

In the literature review, many catalysts reportedly demonstrate a decrease in activity due to the deposition of carbon (coking) on the surface. Compounds which may be precursors of surface coking are carbon monoxide (equation 4.9), methane (equation 4.10), ethylene (equation 4.11), and ethane (equation (4.12).

$$2CO \rightarrow C + CO_2 \quad (4.9)$$

$$CH_4 \rightarrow C + 2H_2 \quad (4.10)$$

$$C_2H_4 \rightarrow 2C + 2H_2 \quad (4.11)$$

$$C_2H_6 \rightarrow 2C + 3H_2 \quad (4.12)$$

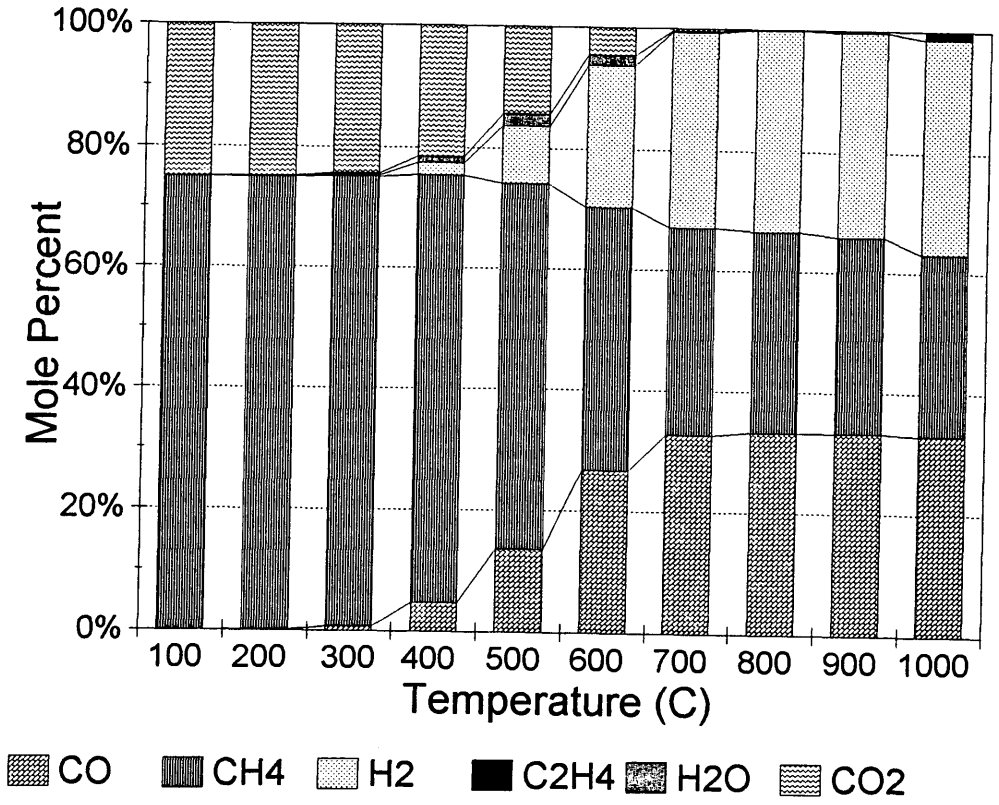

Figure 16. Mole percent of product distribution for simultaneous ethanol decomposition and side reactions, as determined using ASPEN PLUS.

The Gibbs free energy of reaction of reaction (4.9) through (4.12) versus temperature were calculated using the CHETAH (7.0) program. The results are plotted in ***Figure 17***. Carbon formation from ethylene is thermodynamically favorable at all temperatures. Since ethylene is likely to be a by-product of ethanol decomposition, a catalyst must be designed to minimize its production.

In addition, at temperatures lower than 400°C carbon monoxide also has a high feasibility to produce surface carbon at the equilibrium conditions. Because carbon monoxide is one of the products from ethanol decomposition, the reaction may have to be controlled kinetically to prevent the system from approaching equilibrium in which coke formation from carbon monoxide is favorable.

The formation of carbon from ethane and methane have a low feasibility at low temperatures (below 200°C for ethane and below 500°C for methane). However, the feasibility increases as the temperature increases.

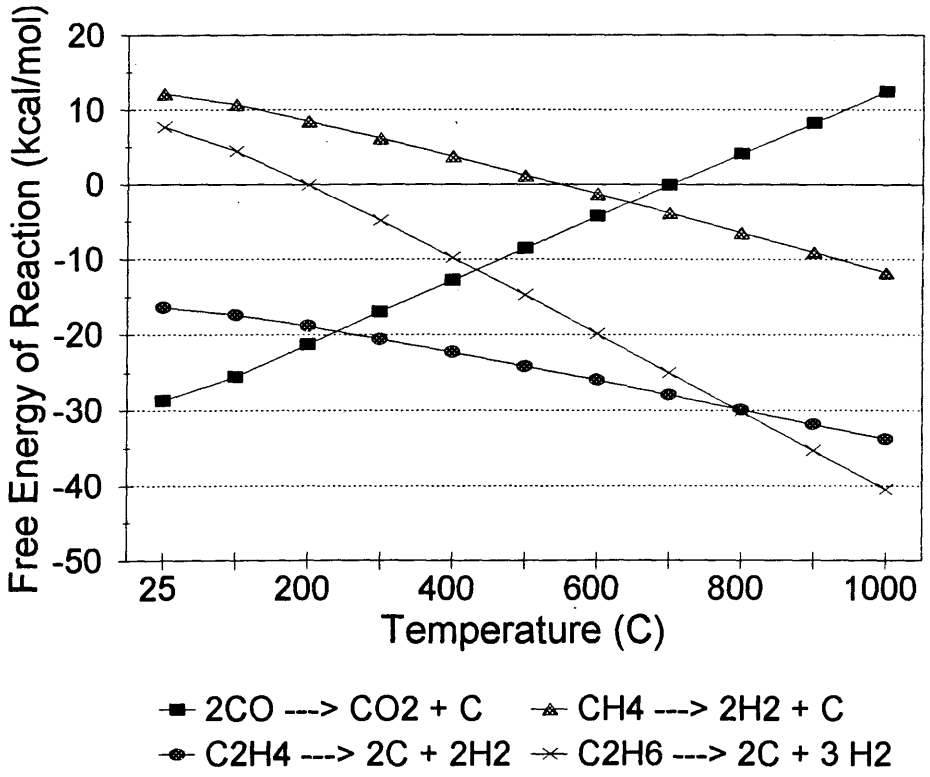

Figure 17. Gibbs free energy of reaction of carbon formation from carbon monoxide, methane, ethylene and ethane.

For on-board applications, temperatures between 100 and 500°C are probably more realistic for the indirect production of cold-start agents. Thermodynamic analysis suggests that methane would be the predominant cold-start agent in this temperature range. Methane is an excellent fuel and would be an acceptable cold-start agent.

The thermodynamic results presented above can not predict how rapidly equilibrium is approached for each of the reactions discussed. The use of a catalyst may have a profound effect on selected reaction rates and markedly alter the product distribution at a given temperature and catalyst contact time. Catalyst activity is defined as a measure of the relative rates at which the system approaches equilibrium. Therefore, a comparison of catalyst activities must be conducted under non-equilibrium conditions. Once the system reaches equilibrium, distinction between catalyst behaviors is lost. The thermodynamic data presented here will also be used to verify that the catalysts are indeed being evaluated at non-equilibrium conditions.

Chapter 5
RESULTS AND DISCUSSION

5.1 Catalyst Evaluation

In a catalytic reactor tube it is possible to have homogeneous gas phase reactions (thermal reactions) and/or heterogeneous surface reactions occurring simultaneously. Surface reactions may occur on the walls of the quartz reactor tube, on the surface of the quartz chips and/or on the surface of the catalyst. Approximately 1.000 gram of quartz chips were mixed with the catalyst material to provide a uniform flow through the catalyst bed and to minimize thermal gradients. Since this study is concerned with the evaluation of catalyst materials, only the catalyst surface reactions are of interest. Therefore, it is important that test conditions be established that minimize or eliminate undesirable gas phase or surface reactions. Tests were conducted with and without the catalyst present in the reactor tube. The test conditions employed are described in detail in ***Section 3.5*** of the ***Experimental Procedure*** section.

Test for Undesirable Gas Phase and Surface Reactions

In this study, 1.000 gram of quartz chips was placed on a porous fritted disk mounted approximately in the center of the quartz reactor tube. The exact location of the fritted disk was selected so as to place the catalyst bed (or quartz chips in this case) in an isothermal zone of the oven, (see ***Appendix 3***). The ethanol pump rate was 1.5 cc/hr, the helium diluent flow was 20cc/min and resulted in a total space velocity of 3.5 hr^{-1}. The product distribution was obtained over a 200 to 500°C temperature range in 100°C increments. The reaction was evaluated for three hours at each temperature. The product distribution was obtained using an on-line gas chromatograph and the results are given in ***Table 2***. The activity and selectivity for ethanol conversion are defined as follows:

$$\% \text{ Activity} = \frac{(\text{Mole EtOH input} - \text{Mole EtOH output}) \times 100}{\text{Mole EtOH input}}$$

$$\% \text{ Selectivity} = \frac{(\text{Desired Reaction}) \times 100}{\text{All Reactions}}$$

$$= \frac{\text{Mole \% CO} \times 100}{\text{Mole \% } [(CH_3CHO) + (CO) + (CO_2) + (C_2H_4) + (C_2H_6)]}$$

No ethanol conversion was observed at 200°C. At 300°C approximately 1.0 mole percent conversion of ethanol to acetaldehyde and hydrogen was observed, see equation (4.2). At these conversion levels, the quantity of hydrogen was too small to be detected by the thermal conductivity detector. Therefore the mole percent of hydrogen was obtained stoichiometrically, i.e. set equal to that of acetaldehyde.

At 400 °C, ethanol conversion to acetaldehyde increased to 2 percent. During the three hours of observation, the activity decreased gradually with time. This suggests that ethanol conversion occurs at the surface of the quartz chips or the walls of the quartz tube rather than by gas phase reactions. The decline in activity is likely due to carbon deposition on the active surfaces. After changing the temperature to 500°C, ethanol conversion reached 3 percent. In addition to acetaldehyde, carbon monoxide and methane were also produced. The later products were most likely due to acetaldehyde decomposition, see equation (4.3). A trace amount of ethylene from ethanol dehydration was also detected, see equation (4.4).

These studies suggest that the relative catalyst activities and selectivities can be safely evaluated between 200 to 500°C. The conversions are small and the contribution to the overall conversions will be minor compared to the conversions expected when the catalyst is added to the reactor tube. Gas phase reactions are expected to become more significant above 500°C. Thus, catalysts were not tested above this temperature. This information will serve as background data and will be subtracted from the activity obtained for tests conducted in the presence of a catalyst. Thus, the reported values will be relative values.

Table 2. Ethanol Reactions without a catalyst

Tested Material: 1.000 g quartz chips

Feed Composition: 1.5 cc/hr ethanol + 20 cc/min helium

Space Velocity: 3.5 hr^{-1}

Temp (C)	H2	CO	CH4	CO2	C2H4	C2H6	H2O	C2H4O	C2H6O	selectivity %	activity %
				Mole % of component							
200	0.00	0.00	0.00	0.00	0.00	0.00	0.00	0.00	100.00		0.00
200	0.00	0.00	0.00	0.00	0.00	0.00	0.00	0.00	100.00		0.00
200	0.00	0.00	0.00	0.00	0.00	0.00	0.00	0.00	100.00		0.00
200	0.00	0.00	0.00	0.00	0.00	0.00	0.00	0.00	100.00		0.00
200	0.00	0.00	0.00	0.00	0.00	0.00	0.00	0.00	100.00		0.00
200	0.00	0.00	0.00	0.00	0.00	0.00	0.00	0.00	100.00		0.00
average	0.00	0.00	0.00	0.00	0.00	0.00	0.00	0.00	100.00		0.00
300	0.74	0.00	0.00	0.00	0.00	0.00	0.00	0.74	98.51	0.00	0.74
300	1.04	0.00	0.00	0.00	0.00	0.00	0.00	1.04	97.91	0.00	1.04
300	1.10	0.00	0.00	0.00	0.00	0.00	0.00	1.10	97.79	0.00	1.10
300	1.17	0.00	0.00	0.00	0.00	0.00	0.00	1.17	97.66	0.00	1.17
300	1.25	0.00	0.00	0.00	0.00	0.00	0.00	1.25	97.50	0.00	1.25
300	1.30	0.00	0.00	0.00	0.00	0.00	0.00	1.30	97.39	0.00	1.30
average	1.10	0.00	0.00	0.00	0.00	0.00	0.00	1.10	97.79	0.00	1.10
400	2.38	0.00	0.00	0.00	0.00	0.00	0.00	2.38	95.24	0.00	2.38
400	2.11	0.00	0.00	0.00	0.00	0.00	0.00	2.11	95.77	0.00	2.11
400	1.76	0.00	0.00	0.00	0.00	0.00	0.00	1.76	96.49	0.00	1.76
400	1.56	0.00	0.00	0.00	0.00	0.00	0.00	1.56	96.89	0.00	1.56
400	1.48	0.00	0.00	0.00	0.00	0.00	0.00	1.48	97.05	0.00	1.48
400	1.40	0.00	0.00	0.00	0.00	0.00	0.00	1.40	97.21	0.00	1.40
average	1.78	0.00	0.00	0.00	0.00	0.00	0.00	1.78	96.44	0.00	1.78
500	2.85	0.05	0.05	0.00	0.26	0.00	0.26	2.80	93.99	1.61	2.90
500	2.45	0.04	0.04	0.00	0.19	0.00	0.19	2.40	94.87	1.52	2.49
500	2.32	0.04	0.04	0.00	0.16	0.00	0.16	2.28	95.16	1.61	2.36
500	2.23	0.00	0.00	0.00	0.15	0.00	0.15	2.23	95.38	0.00	2.23
500	2.29	0.04	0.04	0.00	0.15	0.00	0.15	2.25	95.23	1.64	2.33
average	2.43	0.03	0.03	0.00	0.18	0.00	0.18	2.39	94.93	1.28	2.46

5.2 Ethanol Decomposition over Platinum-Based Catalysts

The supported platinum catalysts prepared and evaluated in this study were 2%Pt/SiO_2, 2%Pt/2%La_2O_3/SiO_2 and 2%Pt/5%La_2O_3/SiO_2. All three catalysts were evaluated at 200, 300, 400 and 500°C, and again at 300°C in the tubular reactor system. The final 300°C study was included to observe catalyst deactivation, if any. The catalyst activities and product distribution for hydrogen, carbon monoxide, methane, carbon dioxide, and acetaldehyde are presented in ***Figures 18*** through ***25***, and the complete product analysis is given in ***Appendix 4.***

5.2.1. Ethanol Decomposition at 200°C

At 200°C, the primary reaction was the dehydrogenation of ethanol to acetaldehyde and hydrogen. The average conversions were 2, 12 and 15 % over 2%Pt/SiO_2, 2%Pt/2%La_2O_3/SiO_2 and 2%Pt/5%La_2O_3/SiO_2 ,respectively (see ***Figure 18***). A small amount , less than 5 mole % of the total product, due to acetaldehyde decomposition to carbon monoxide and methane was also observed. Thus, the selectivity was very low, ranging from 5 to 6 percent. For details, see ***Tables A4-1*** through ***A4-3*** in ***Appendix 4.*** No products were observed that could be attributed to the ethanol dehydration reactions, (see equation 4.4 and 4.5), nor the water gas shift reaction, (equation 5.7). The primary products were hydrogen and acetaldehyde, see ***Figure 19***.

Apparently, the activation energy for ethanol dehydrogenation (equation 4.2) is significantly lower than that for acetaldehyde decomposition (equation 4.3). ASPEN PLUS thermodynamic calculations predict only methane and

carbon dioxide as products at this temperature. It is obvious that the combined reactions are displaced far from thermodynamic equilibrium and that the reactions are kinetically controlled, compare ***Figures 16*** and ***19***.

It is important to note that the lanthana modified silica supports produced catalysts that were significantly more active than the unmodified silica support. This may due to increased dispersion of the platinum metal (smaller crystallites) or possibly to a strong metal-support interaction (SMSI) between the lanthana modifier and the platinum metal.

5.2.2 Ethanol Decomposition at 300°C

Increasing the temperature to 300°C resulted in a marked increase in catalyst activity. For details see ***Tables A4-1*** through ***A4-3*** in ***Appendix 4***. The catalysts demonstrated average conversions of 33, 85 and 89 and average selectivities of 29, 49 and 56 for the 2%Pt/SiO_2, 2%Pt/2%La_2O_3/SiO_2 and 2%Pt/5%La_2O_3/SiO_2, catalysts as shown in ***Figure 20***. These results suggest that the acetaldehyde decomposition is now occurring at a significant rate, as evidence by a marked increase in hydrogen, methane and carbon monoxide production relative to acetaldehyde, (see ***Figure 21***). Only a trace amount of carbon dioxide was observed indicating that the water-gas shift reaction is not important at this temperature. Since no dehydration products were observed, the source of water for this reaction must come from the small amount of impurity observed in the original feed stock. The product distribution is still far from the calculated thermodynamic equilibrium, again indicating that the reactions are kinetically limited.

The effect of lanthana at this temperature is similar to that at 200°C. The

catalysts employing lanthana-modified support are significantly more active than the unmodified counterpart. This results in an increase in both ethanol dehydrogenation and acetaldehyde decompositions. However, all three catalysts showed a gradual decline in acetaldehyde decomposition over the three hour testing period. This suggests that some catalyst deactivation was occurring, see ***Figure 20***. Trace amount of ethylene and ethane were detected. The presence of ethylene suggests that the catalyst retains sufficient acidity at this temperature to promote a small amount of ethanol dehydration. In addition, it was observed that the products of ethanol dehydration were slightly increased with increasing lanthana loading. This increase could be caused by either the increase in lanthana loading or by the increase in metal dispersion. From these data, it is possible to distinguish between the two possible causes. Determination of the effect of lanthana on catalyst acidity and the potential of ethanol dehydration on pure platinum metal are recommended for future study.

5.2.3 Ethanol Decomposition at 400°C

The catalyst conversions and selectivities were optimized at 400°C, where conversions were 100 percent, (see ***Figure 22***) and selectivities ranged between 94 and 92 percent. The decline in the selectivity with increasing lanthana loading is accompanied by an increase of carbon dioxide production. The predominant reaction products were hydrogen, methane and carbon monoxide (see ***Figure 23***). At this temperature acetaldehyde decomposition was nearly complete on 2%Pt/SiO_2, and complete on 2%Pt/2%La_2O_3/SiO_2 and 2%Pt/5%La_2O_3/SiO_2. All three catalysts gave essentially same product distribution. The 2%Pt/SiO_2 catalyst showed a gradual loss in activity for both

the ethanol dehydrogenation and acetaldehyde decomposition reactions. The catalysts using lanthana modified supports showed no significant loss in activity over the duration of the evaluation. Ethanol dehydration to form ethylene occurred to a slightly higher extent over the 2% lanthana modified support than the unmodified support. The 2%Pt/5%La_2O_3/SiO_2 catalyst showed no trace of ethylene; however, a trace of ethane was observed. It may be possible that this catalyst prevents ethylene formation or promotes ethylene hydrogenation to ethane.

As shown in the product analysis in ***Tables A4-1*** through ***A4-3*** in ***Appendix 4***, the mole percent of carbon monoxide was lower than that of methane in all three catalysts. Thus, it is likely that the trace amount of carbon dioxide was formed from carbon monoxide via the water-gas shift reaction. This can be explained by the result of the previous thermodynamic calculations which indicated that this reaction is thermodynamically favorable at this temperature.

5.2.4 Ethanol Decomposition at 500°C

As shown in ***Figures 24*** and ***25***, all catalysts conversions were lower at 500°C than those observed at 400°C. It is obvious that catalyst deactivation occurred rapidly at this temperature. Both ethanol dehydrogenation and acetaldehyde decomposition showed a rapid decline during the test period. However, the unmodified support deactivated to a greater extent than the modified supports. The initial activity over the Pt/SiO_2 catalyst must have been close to 100%, but rapidly deactivated to 12.64% by the time the first sample was analyzed. The catalyst deactivation is most likely caused by ethylene polymerization, by acetaldehyde polymerization or by carbon monoxide

disproportionation which eventually forms an inactive carbon layer on the metal surface; this process is referred to as catalyst coking. Since acetaldehyde, but not ethylene, was observed at 300°C, and no significant deactivation was observed, it is unlikely that acetaldehyde is the primary source of catalyst deactivation. Carbon monoxide is present in large amounts at both 300 and 400°C and no significant deactivation was observed during in the test period. Therefore, carbon monoxide disproportionation is also eliminated as the primary coking process. The catalyst activity should asymptotically approach zero as coking progresses, and indeed this is the case, (see ***Figure 24***). The lanthana modified supports appear to asymptotically approach zero activity at a different rate than the unmodified support. In fact, it is possible that all the catalysts will reach some non-zero steady state value. A non-zero steady state activity would suggest that some mechanism exist for the slow removal of carbon. As the catalyst activity declines the carbon formation rate also declines until the carbon formation and carbon removal rates are equal. Possible carbon removal reactions could include the hydrogenation of carbon to produce methane and/or the oxidation of carbon by water to produce methane. From ***Figure 17***, carbon hydrogenation, which is the reverse reaction of coke formation from methane, is thermodynamically favorable between 200 and 500°C.

XRD analyses of both fresh and tested catalysts show the lanthana modified catalysts have a higher dispersion of the platinum metal and thus a higher initial activity per gram of catalyst would be expected. However, all the catalysts would be expected to reach the same steady state activity. The asymptotic approach to this steady state value would be displaced according to the increase in available metal surface atoms. If the lanthana modified catalysts reach a higher steady state value than the unmodified catalyst, then the metal

surface atoms in the modified catalysts must have a higher activity for the carbon removal reaction. This would suggest the presence of a strong metal-support interaction between the platinum and the lanthana modifier which alters the activity of the platinum metal atoms.

5.2.5 Ethanol Decomposition at 300°C, Test for Deactivation

At the end of the three hour test period at 500°C, the reactor temperature was reduced to 300°C. These results can be compared to the initial test conducted at 300°C, (see ***Figures 20*** and ***21***). As shown in ***Tables A4-1*** through ***A4-4*** in ***Appendix 4***, all three catalysts showed almost complete loss of activity. A residual activity of ethanol dehydrogenation was still observed, but all activity of acetaldehyde decomposition was lost. All three catalysts showed severe signs of coking. It is apparent that the catalyst deactivation is caused primarily by ethylene polymerization and subsequent coke formation on the metal surface. The degree of catalyst deactivation appears to correlate with the amount of ethylene produced during the reaction. Acetaldehyde polymerization was also considered to be a possible source of deactivation, but there is no clear correlation between deactivation and the amount of acetaldehyde in the product.

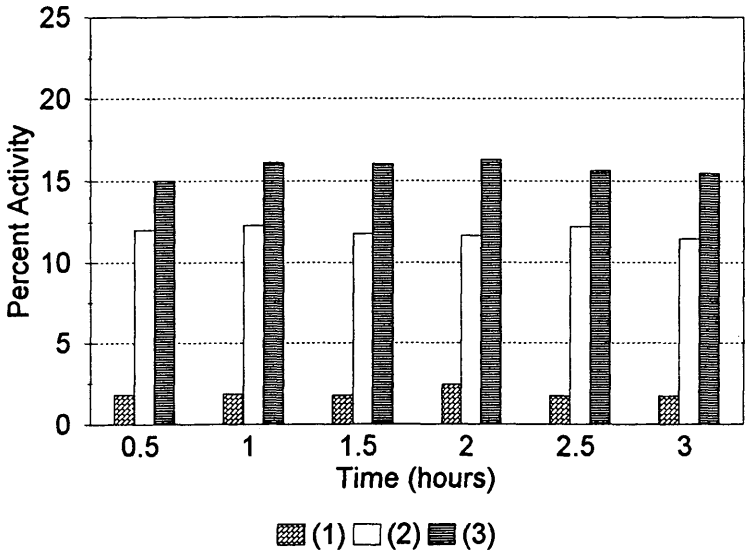

Figure 18. The activities of (1) 2%Pt/SiO_2, (2) 2%Pt/2%La_2O_3/SiO_2 and (3) 2%Pt/5%La_2O_3/SiO_2 at 200°C.

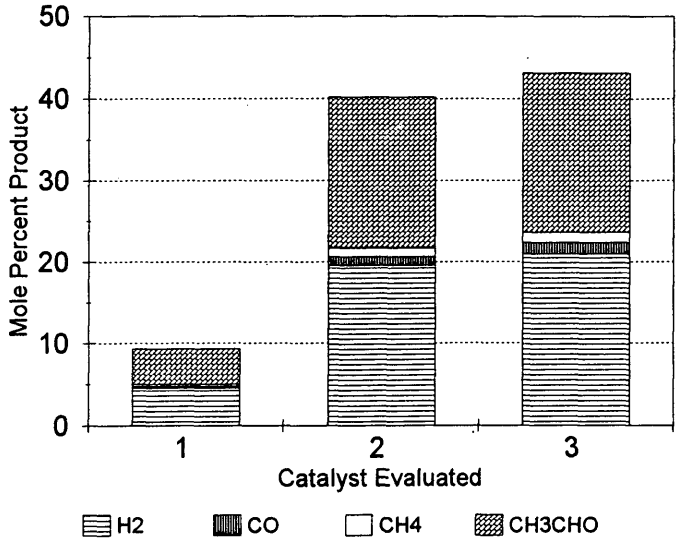

Figure 19. Product distribution for ethanol decomposition over (1) 2%Pt/SiO_2, (2) 2%Pt/2%La_2O_3/SiO_2 and (3) 2%Pt/5%La_2O_3/SiO_2 at 200°C.

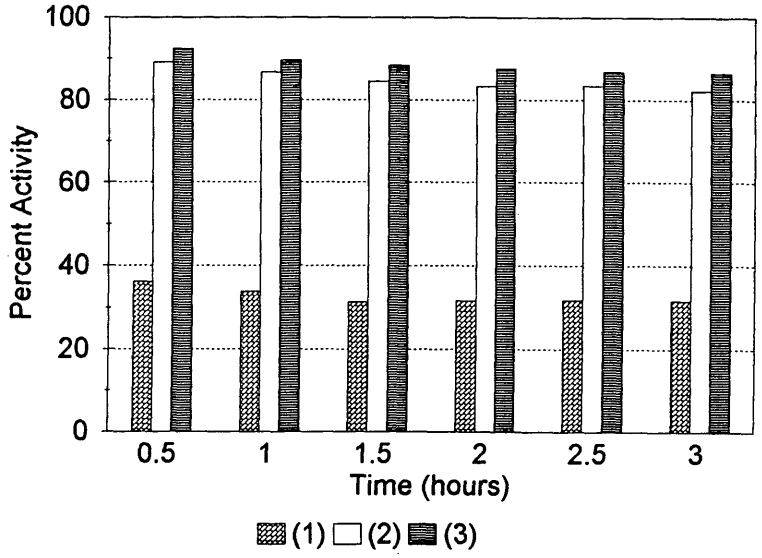

Figure 20. The activities of (1) 2%Pt/SiO_2, (2) 2%Pt/2%La_2O_3/SiO_2 and (3) 2%Pt/5%La_2O_3/SiO_2 at 300°C.

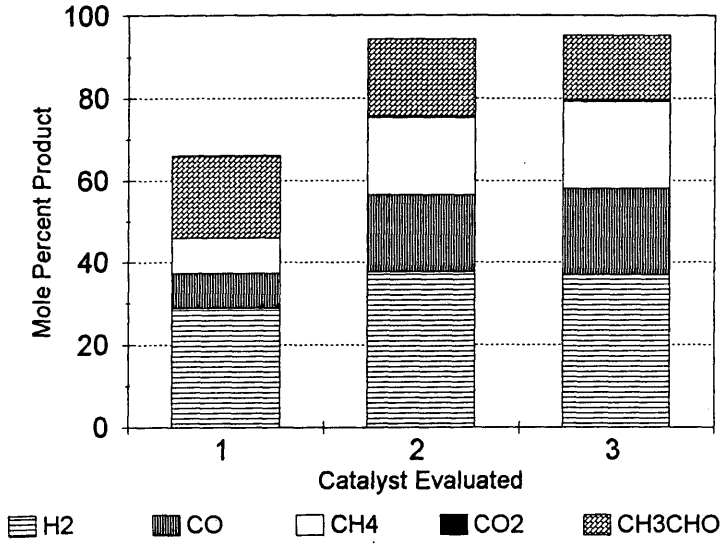

Figure 21. product distribution for ethanol decomposition over (1) 2%Pt/SiO_2, (2) 2%Pt/2%La_2O_3/SiO_2 and (3) 2%Pt/5%La_2O_3/SiO_2 at 300°C.

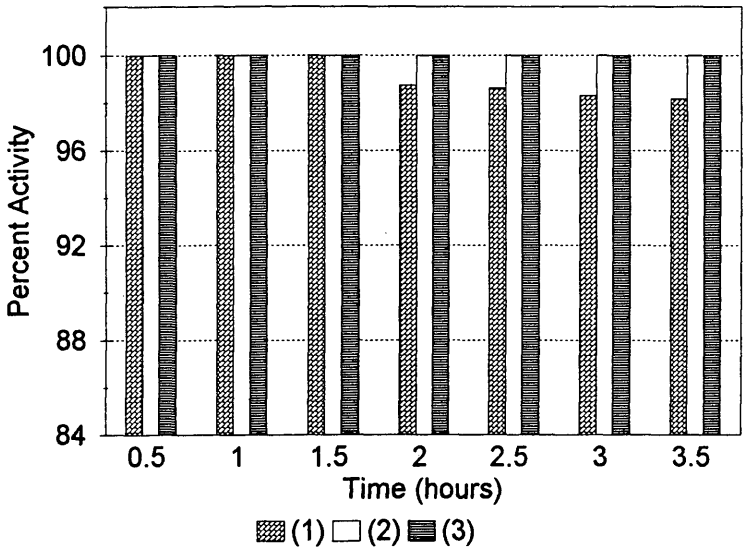

Figure 22. The activities of (1) 2%Pt/SiO_2, (2) 2%Pt/2%La_2O_3/SiO_2 and (3) 2%Pt/5%La_2O_3/SiO_2 at 400°C.

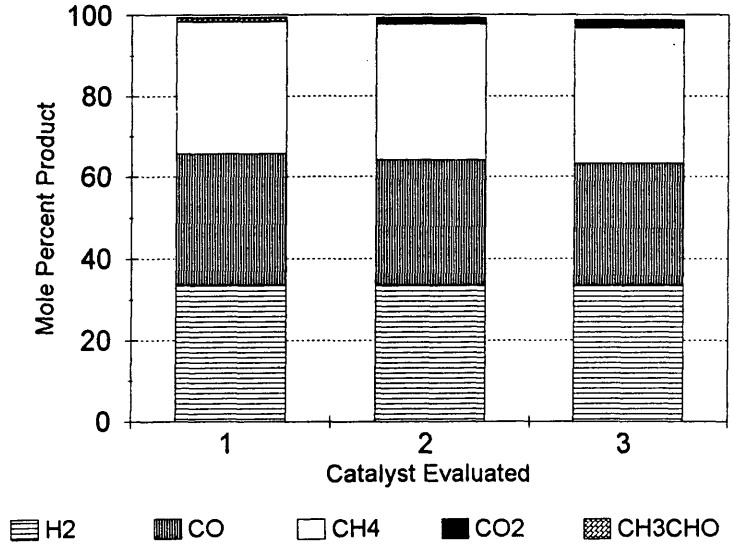

Figure 23. Product distribution for ethanol decomposition over (1) 2%Pt/SiO_2, (2) 2%Pt/2%La_2O_3/SiO_2 and (3) 2%Pt/5%La_2O_3/SiO_2 at 400°C.

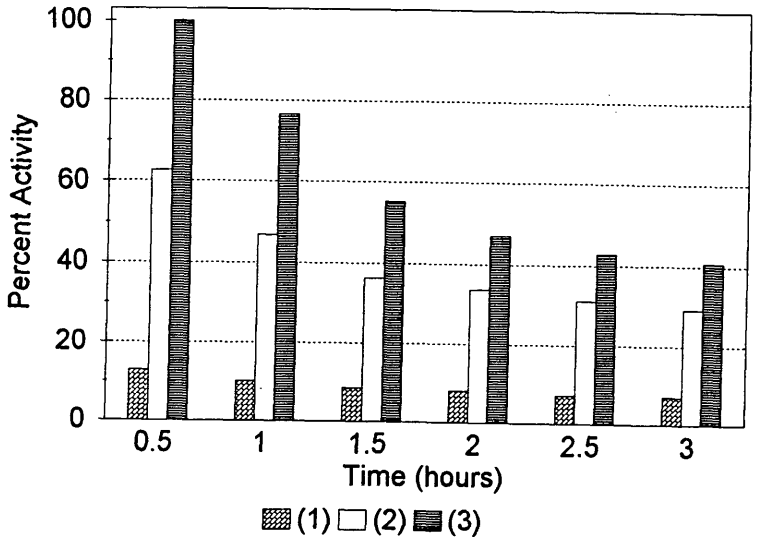

Figure 24. The activities of (1) 2%Pt/SiO_2, (2) 2%Pt/2%La_2O_3/SiO_2 and (3) 2%Pt/5%La_2O_3/SiO_2 at 500°C.

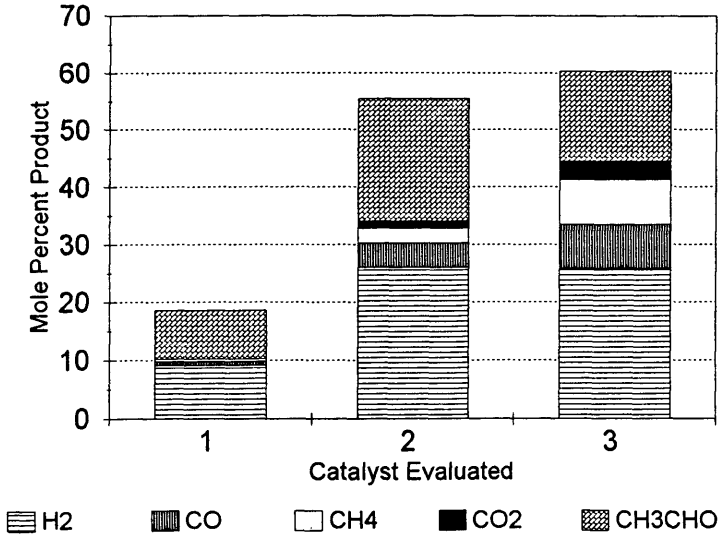

Figure 25. Product distribution for ethanol decomposition over (1) 2%Pt/SiO_2, (2) 2%Pt/2%La_2O_3/SiO_2 and (3) 2%Pt/5%La_2O_3/SiO_2 at 500°C.

5.2.6 Acetaldehyde Decomposition Studies

Pure acetaldehyde was passed over the catalyst at 400°C to determine if it was involved in the coking process. This 2%Pt/5%La_2O_3/SIO_2 catalyst was chosen because it demonstrated the highest activity for the ethanol decomposition reaction. The initial decomposition activity was much lower than expected, only 51.19% compared to 100% when pure ethanol was used under identical reaction conditions. The activity declined rapidly after the first observation (see ***Table 3***). It was apparent that acetaldehyde is involved in the deactivation observed. The rapid deactivation rate may be due in part to the lower partial pressure of hydrogen in this test. In addition, there was a small amount of ethylene produced, and it may have been responsible for some of the observed deactivation. A small amount of ethanol was formed via the hydrogenation of acetaldehyde and it may have served as the source of ethylene.

In summary, the magnitude of the contribution of acetaldehyde to catalyst deactivation remains unclear. The use of pure acetaldehyde resulted in a rapid and severe deactivation of the catalyst. This degree of deactivation was not observed when ethanol was used as the feedstock, even though acetaldehyde is clearly present as a product. The major difference is the much lower hydrogen partial pressure used in the acetaldehyde test. The additional hydrogen may be necessary to retard the acetaldehyde polymerization rate. The small amount of ethylene in the product may have contributed to the deactivation as well.

Table 3. Acetaldehyde decomposition over 2%Pt/5%La_2O_3/SiO_2 at 400 °C.

Tested Material: 0.400 g of 2%Pt/5%La_2O_3/SiO_2 + 1.000 g quartz chips

Feed Composition: 0.75 cc/hr acetaldehyde + 20 cc/min helium

Space Velocity: 2.0 hr^{-1}

Temp	Mole % of component									selectivity	activity
(C)	H2	CO	CH4	CO2	C2H4	C2H6	H2O	C2H4O	C2H6O	%	%
400	11.27	11.27	12.96	2.12	0.00	0.00	0.00	61.77	0.61	80.50	51.19
400	3.54	3.31	3.54	0.41	0.07	0.00	0.07	88.63	0.43	78.44	14.98
400	2.90	2.43	2.90	0.63	0.15	0.00	0.15	90.50	0.34	68.45	12.55
400	2.79	2.56	2.79	0.85	0.10	0.00	0.10	90.01	0.80	59.40	12.88
400	2.34	1.98	2.34	0.74	0.11	0.00	0.11	92.16	0.22	64.92	10.29
averag	4.57	4.31	4.91	0.95	0.09	0.00	0.09	84.61	0.48	70.34	20.38

Comment : The catalyst deactivated faster than when ethanol was a feedstock and after testing, the catalyst and the reactor tube showed a severe coking.

5.3 Ethanol Decomposition over Palladium-Based Catalysts

Palladium-based catalysts are more active than platinum-based ones for methanol decomposition. Therefore, 2%Pd/SiO_2 and 2%Pd/5%La_2O_3/SiO_2 catalysts were also studied for the ethanol decomposition reaction. The results are given in ***Tables A4-4*** and ***A4-5*** in ***Appendix 4***. Both catalysts demonstrated much poorer activity than the platinum catalyst. At 200°C the conversions on both catalysts were less than 2 percent. Both ethanol dehydrogenation and acetaldehyde decomposition were observed. Approximately 70% of acetaldehyde from ethanol dehydrogenation underwent decomposition. The conversions were increased at 300°C to 14 percent and 31 percent over 2%Pd/SiO_2 and 2%Pd/5%La_2O_3/SiO_2, respectively (see ***Figure 28***). These results indicated that lanthana also improved activity in palladium catalysts. Ethanol dehydration and carbon monoxide stream reforming were not observed on these catalysts at 200 and 300°C. The product distribution over these catalysts is shown in ***Figure 27***.

After increasing the temperature to 400°C, both catalysts showed a rapid loss in activity. However, as shown in ***Table A4-4*** and ***A4-5*** of ***Appendix 4***, the deactivation of the 2%Pd/5%La_2O_3/SiO_2 catalyst was much slower than that of the 2%Pd/SiO_2 catalyst. This suggests that lanthana has a similar effect on both the platinum and palladium metals with respect to enhancement of activity. Although the testing time was shorter, the palladium catalysts were more severely coked than the platinum catalysts. The reason for the rapid rate of coking relative to platinum is unclear, since both ethylene and acetaldehyde relative concentrations are lower for the palladium catalyst. This would suggest that the carbon removal reactions are very important in determining the overall

deactivation rate and that palladium has a poor activity for this process.

In summary, the palladium catalyst shows a lower ethanol dehydrogenation, a higher acetaldehyde decomposition, and a higher deactivation rate relative to platinum. This results in an overall lower catalyst activity but a higher selectivity.

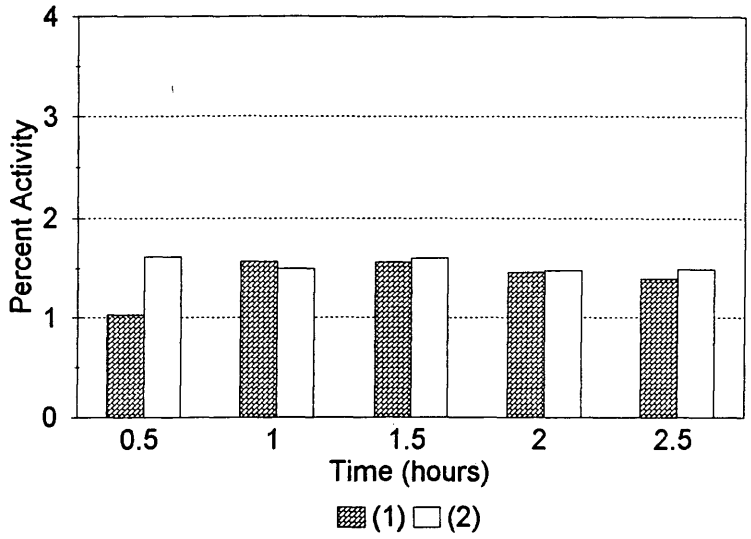

Figure 26. The activities of (1) 2%Pd/SiO_2 and (2) 2%Pd/5%La_2O_3/SiO_2 at 200°C.

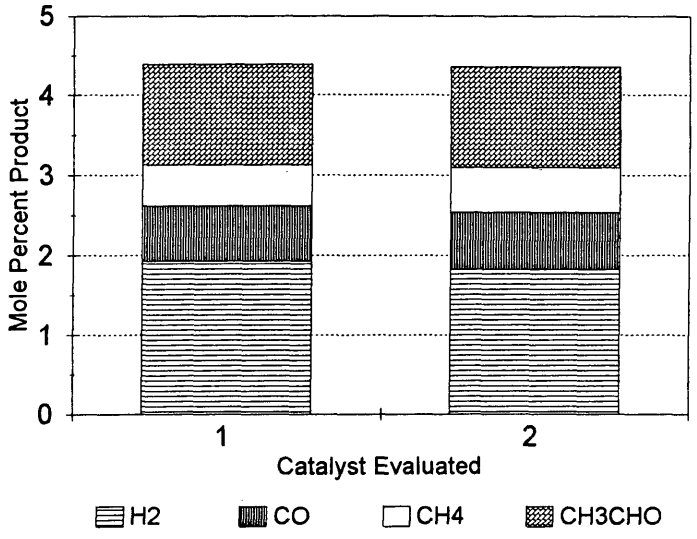

Figure 27. Product distribution for ethanol decomposition over (1) 2%Pd/SiO_2 and (2) 2%Pd/5%La_2O_3/SiO_2 at 200 °C.

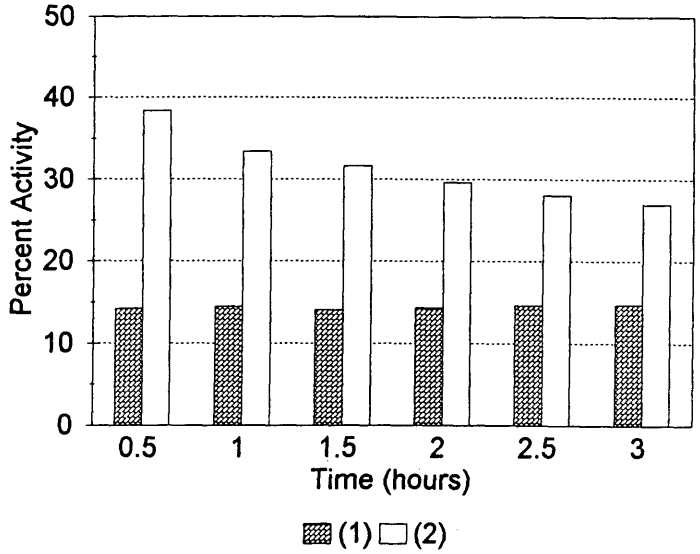

Figure 28. The activities of (1) 2%Pd/SiO_2 and (2) 2%Pd/5%La_2O_3/SiO_2 at 300°C.

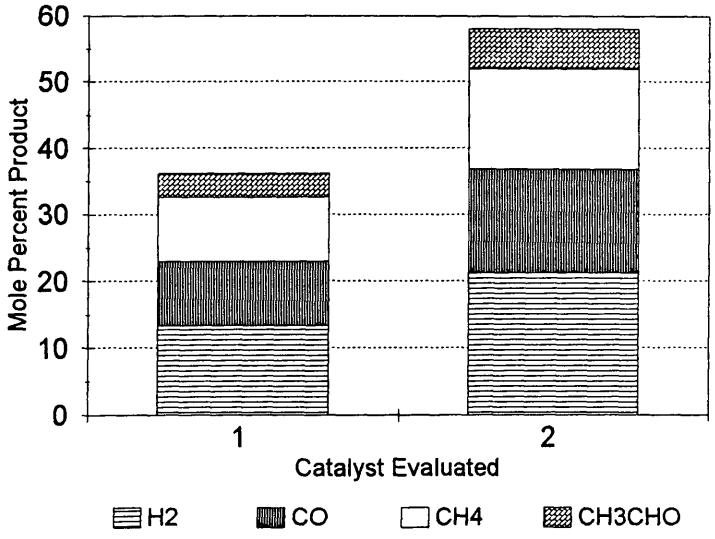

Figure 29. Product distribution for ethanol decomposition over (1) 2%Pd/SiO_2, and (2) 2%Pd/5%La_2O_3/SiO_2 at 300 °C.

5.4 Surface Mechanism for Ethanol Decomposition Reactions

Based on the product distributions observed during the catalyst test phase of this study and information obtained from other published work, the following mechanistic sequence is proposed for ethanol dehydrogenation, acetaldehyde decomposition, ethane formation, ethylene formation, and carbon dioxide formation reactions, (see ***Figures 30*** through ***34***).

From the literature review, ethanol dissociatively adsorbs to the surface in the form of surface ethoxy and hydrogen as shown in ***Figure 30***. The adsorbed ethoxy then loses another hydrogen from the $-CH_2-$ group and desorbs as acetaldehyde. Hydrogen gas is formed from the recombination of the two surface hydrogens. The dehydrogenation reaction in the presence of platinum or palladium-based catalysts was significantly higher than that in the absence of a catalyst. Thus, these metals help to reduce the activation energy for the above reactions.

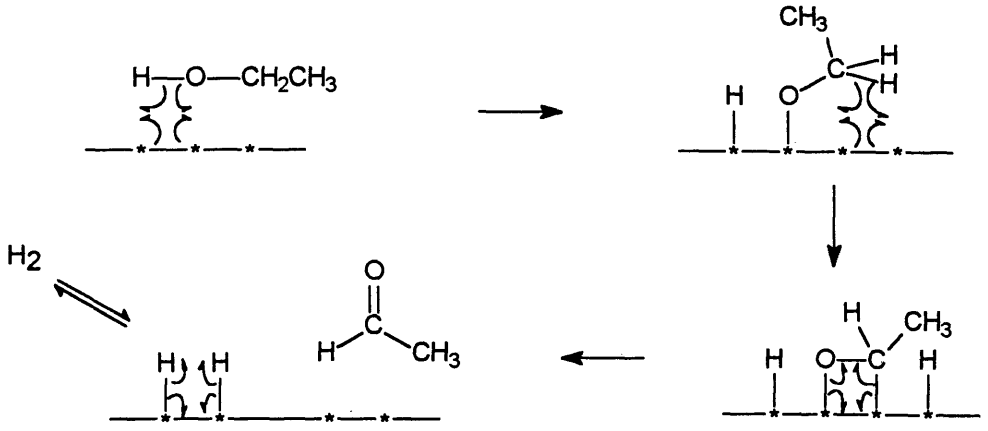

Figure 30. A proposed mechanism of ethanol dehydrogenation on the surface.

On the platinum-based catalysts, ethanol dehydrogenation was favored over acetaldehyde decomposition at 200°C. This indicates that the first reaction has a lower activation energy than the second, even though the second reaction is thermodynamically favored. As proposed in ***Figure 31***, acetaldehyde is likely attached to the metal surface via cleavage of the carbonyl π bond to form an associatively adsorbed species. Since adsorption and desorption reactions are typically fast compared to surface reactions, it is assumed that associatively adsorbed acetaldehyde is in equilibrium with acetaldehyde molecules in the gas phase. A slower surface reaction results in the decomposition of the associatively adsorbed acetaldehyde species into an adsorbed acetyl species and a surface hydrogen. Cleavage of the C-C bond in the acetyl species results in the formation of surface carbon monoxide and methyl species. And finally, the methyl species combines with atomic surface hydrogen to form methane. At 300 and 400°C, the acetaldehyde decomposition was dominant, suggesting that the reaction is approaching thermodynamic equilibrium.

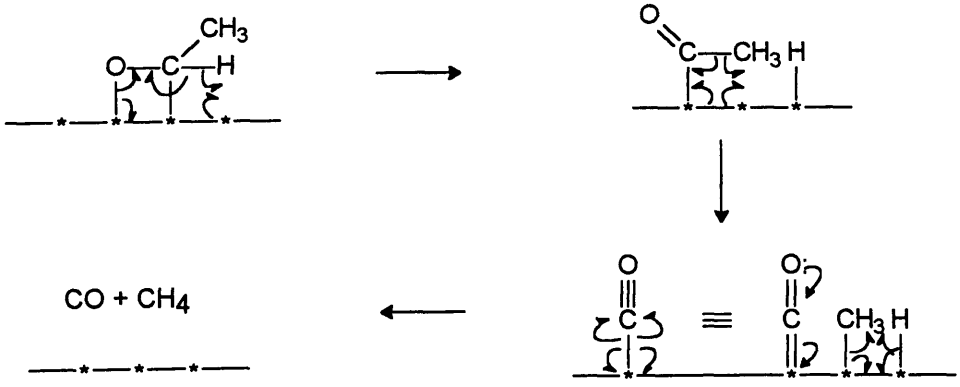

Figure 31. A proposed mechanism of acetaldehyde decomposition on the surface.

Ethylene can be formed by dehydration of ethanol over an acidic surface, such as the silica support, (see ***Figure 32***). In this study the silica supports were modified with a coating of lanthana in an attempt to remove all or most of the surface acidity. The formation of ethylene suggests that either some residual acidity remains on the support or ethylene formation occurs on the metal surface via the mechanism shown in ***Figure 33***. Ethanol dissociatively adsorbs through the cleavage of the C-O bond to form surface ethyl and hydroxy. Then the surface ethyl loses one hydrogen from the methyl group and finally desorbs as ethylene. The surface hydroxy reacts with surface hydrogen and desorbs as water. One possible way to resolve the relative contribution of ethylene formation by the two materials is to study the dehydration reaction on the two materials separately, i.e. the modified lanthana modified silica support or the metal. This test was not done because of time constraints but would be of interest in the future.

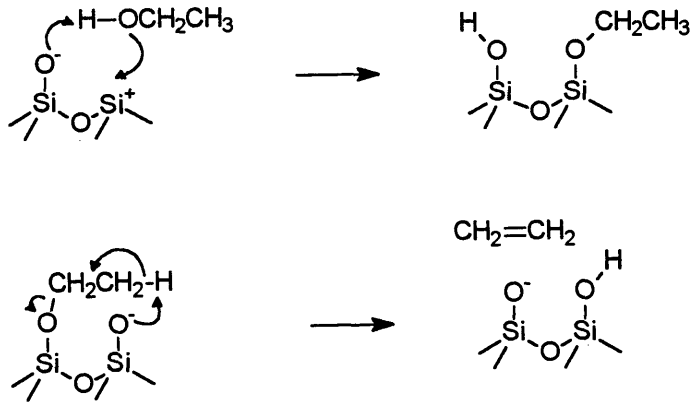

Figure 32. A proposed mechanism of ethanol dehydration on the acidic surface

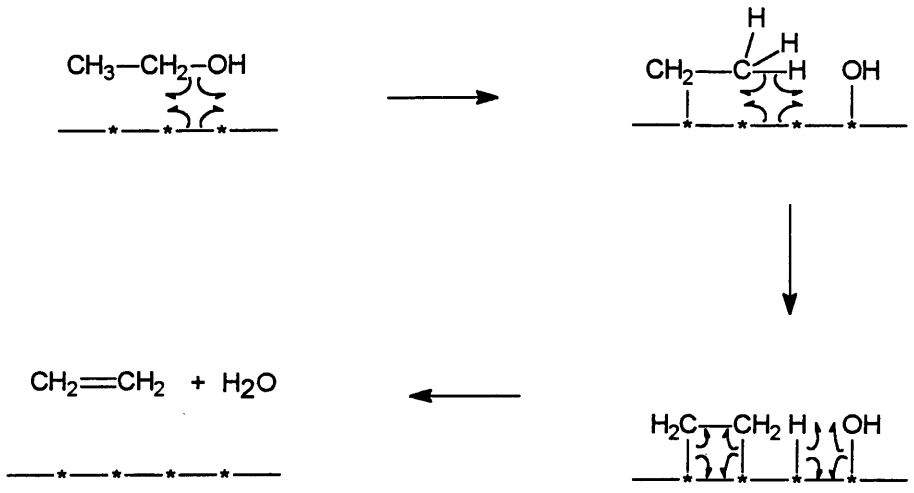

Figure 33. A proposed mechanism of ethylene formation on the surface.

There are two possible routes of ethane formation. The first route involves the direct hydrogenolysis of C-O bond to form the ethyl and hydroxyl surface species shown in ***Figure 34 a***. The ethyl and hydroxyl species combine with atomic surface hydrogen to give ethane and water. The second route occurs via hydrogenation of ethylene, see ***Figure 34 b***. This mechanism involves the formation of an associative adsorbed ethylene species and its subsequent combination with atomic surface hydrogen to produce ethane.

a

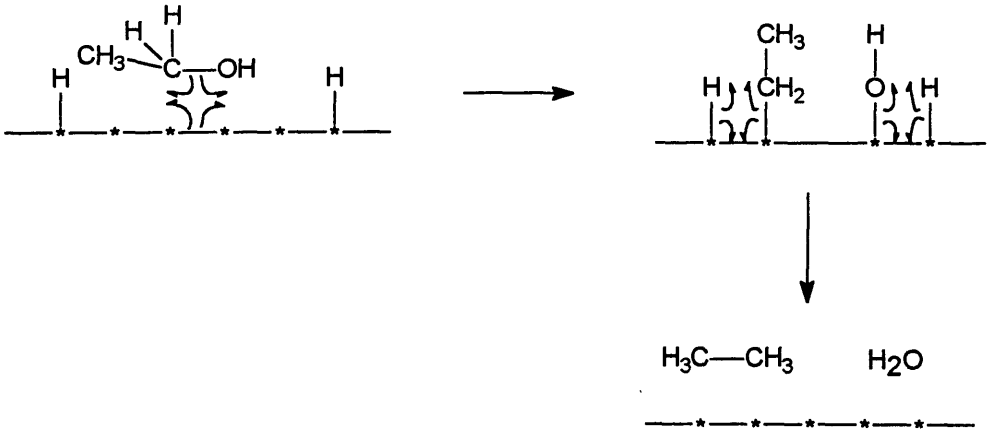

b

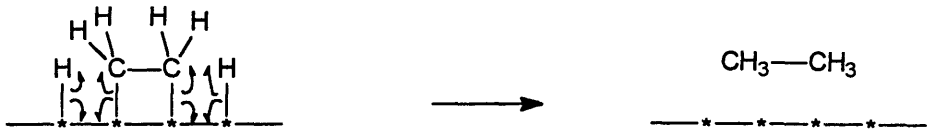

Figure 34. A proposed mechanism of ethane formation on the surface.

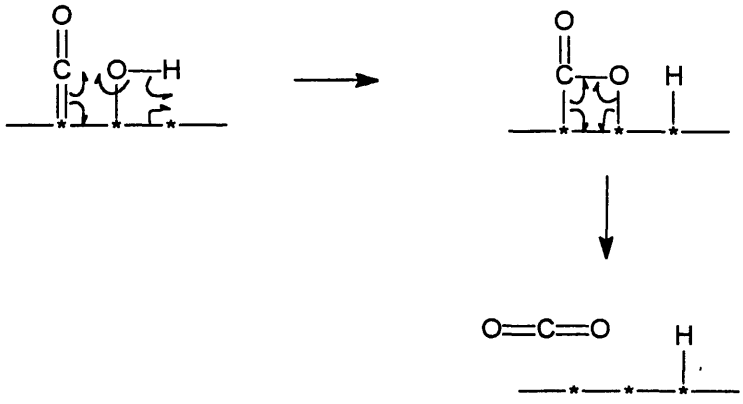

Figure 35. A proposed mechanism of carbon dioxide formation on the surface.

Figure 35 proposes a possible route of carbon dioxide formation from the surface carbonyl (the precursor of carbon monoxide) and surface hydroxy.

5.5 Catalyst Characterization by X-ray Powder Diffraction

The catalysts used for the testing of ethanol decomposition were prepared by impregnating silica or lanthana-modified silica supports with a solution of the platinum or palladium salt and calcining at 550°C in air. Before testing, catalysts were reduced by hydrogen at a flow rate of 30 ml/min at 400°C for two hours in order to produce the active metal. X-ray powder diffraction (XRD) was used to identify the crystalline phases present in the freshly calcined and tested catalysts. In addition, the average crystallite diameter of supported metal crystallites was determined using a line broadening method. Catalysts

with a higher metal dispersion (or smaller metal crystallite diameters) were expected to have higher activity for ethanol decomposition, due to an increase the metal surface area. The XRD line pattern for a SiO_2 support, pure La_2O_3, a $2\%La_2O_3/SiO_2$ support, and a $5\%La_2O_3/SiO_2$ support are shown in ***Figures 36*** and ***37***. The SiO_2, $2\%La_2O_3/SiO_2$, and $5\%La_2O_3/SiO_2$ show a single broad peak at approximately 22 degrees 2θ, which is characteristic of the short range order present in amorphous silica. There was no evidence of crystalline La_2O_3 present on the $2\%La_2O_3/SiO_2$ support. However, a very broad shoulder was observed for the $5\%La_2O_3/SiO_2$ sample at approximately 26 degrees 2θ, which might correspond to the largest peak in the La_2O_3 line pattern. Assuming that the lanthana molecule is planar, the percent area of silica covered by lanthana is 3.4 and 8.7% in the $2\%La_2O_3/SiO_2$, and $5\%La_2O_3/SiO_2$, respectively (see ***Appendix 5***). The line pattern for pure crystalline La_2O_3 has peaks at 16, 26.2, 27, 39.5 and 49 degrees 2θ. The lack of a crystalline pattern for La_2O_3 indicates it is highly dispersed over the SiO_2 surface, perhaps as a partial monolayer or has decomposed to an amorphous $La_2(SiO_3)_3$ or similar silicate.

XRD patterns for the fresh and tested catalysts, ***Figures 39*** through ***44***, were compared to those of the pure platinum and palladium metal standards, shown in ***Figure 38***. The major diffraction lines of platinum are at 40.0, 46.8, 68.2, 82.0 and 86.4 degrees 2θ, while those of palladium are at 39.8, 46.4, 67.9, 81.9 and 86.5 degree 2θ. The diffraction pattern for palladium oxide was obtained from the American Society for Testing Material (ASTM) Powder Diffraction File. The major lines are at 33.8, 42.0, 54.8, 60.7 and 71.4 degrees 2θ.

The XRD line patterns of the freshly calcined and tested platinum-based catalysts are shown in ***Figures 39*** through ***41***. The $2\%Pt/SiO_2$ catalyst showed

a crystalline line pattern for platinum metal for both the fresh and tested samples. The average crystallite diameters calculated from the line broadening method were 391.4 and 590.2 A° for the freshly calcined and tested catalysts, respectively. The ratio of the platinum peak at 40 degrees 2θ to the broad SiO_2 peak at 22 degrees 2θ for the fresh catalyst is 1.42 while the tested catalyst has a ratio of 1.96. These values suggest that some sintering of the metal has occurred during the reduction and testing sequence. The proposed surface picture of 2%Pt/SiO_2 is shown in ***Figure 42a***. The platinum crystallites on silica are large enough to be detected by XRD analysis, resulting in narrow metal peaks. This indicates that the interaction between platinum and silica is not strong.

The XRD patterns of the freshly calcined and tested 2%Pt/2%La_2O_3/SiO_2 and 2%Pt/5%La_2O_3/SiO_2 catalysts were essentially identical. In the freshly calcined catalysts, no platinum metal peaks were observed. This result suggests the platinum exists as crystallites smaller than 10Å (the lower limit of the XRD line broadening method) or is monoatomically dispersed on the SiO_2 surface or has formed an amorphous silicate. Comparing the line pattern for the fresh 2%Pt/SiO_2 sample to that of the 2%Pt/2%La_2O_3/SiO_2 and 2%Pt/5%La_2O_3/SiO_2 samples, it can be concluded that lanthana greatly improves the metal dispersion, for example compare ***Figures 39*** and ***40***. Since platinum oxide is not thermodynamically stable at the 500°C calcining temperatures used, it was assumed that all the platinum existed in the metal phase. The high degree of dispersion of a non-polar metal on a polar oxide support is unexpected. This would suggest a very strong interaction exists between the platinum metal and the lanthana surface or that a species other than platinum metal exists. The proposed surface picture of these catalysts is

shown in ***Figure 42b***. The narrow line pattern for platinum peaks observed for the 2%Pt/SiO_2 catalyst were not observed from the 2%Pt/2%La_2O_3/SiO_2 and 2%Pt/5%La_2O_3/SiO_2 catalysts. The lanthana modifier only occupies 3-8% of the silica surface, (see ***Appendix 5***). The absence of large platinum crystallites, which is characteristic of platinum on silica, suggests the bulk of the platinum is strongly associated with the lanthana modifier and not the silica. XRD analysis of the reduced and tested catalyst samples showed the presence of broad platinum metal peaks for both the 2%Pt/2%La_2O_3/SiO_2 and 2%Pt/5%La_2O_3/SiO_2 samples, see ***Figures 40*** and ***41***. The appearance of a platinum metal pattern after reduction and testing of the sample may be due to some metal sintering or to additional reduction of a surface stabilized platinum oxide to platinum metal. XRD cannot distinguish between these two possibilities. The average crystallite diameters were 52.1 and 38.4 A° for the 2%Pt/2%La_2O_3/SiO_2 and 2%Pt/5%La_2O_3/SiO_2 catalysts respectively, see ***Table 4*** for a comparison of crystallite diameters of the tested samples.

In summary, the use of lanthana as a coating on the silica surface greatly improved the platinum metal dispersion which results in a substantially higher metal surface area. This result agreed well with catalyst testing results, in which the activity of the 2%Pt/5%La_2O_3/SiO_2 catalyst was significantly higher than the 2%Pt/SiO_2 catalyst.

The XRD patterns of palladium supported catalysts, which are shown in ***Figures 43*** through ***45***, were not similar to that of platinum. The freshly calcined support catalysts show palladium is present as an oxide phase. Unlike platinum, palladium does form a thermodynamically stable oxide under the calcining conditions used. The XRD patterns of freshly calcined catalysts were similar in all three catalysts, showing very broad lines characteristic of highly dispersed

palladium oxide. A highly dispersed palladium oxide is expected because a polar oxide would be expected to wet the polar surface of a silica or lanthana rather than aggregating into an approximate spherical shape. The opposite would be true for a non-polar metal on a polar support. As a result, the XRD pattern of palladium oxide on silica looks similar to that of palladium oxide on lanthana modified silica. After reducing with hydrogen and testing, all palladium oxide was converted to the palladium metal phase. The average crystallite diameters of palladium on $5\%La_2O_3/SiO_2$ and on silica supports were 99.1 and 110.0 Å, see ***Table 4***. Thus, modification of silica with lanthana also improves the dispersion of palladium.

Table 4. Calculated average crystallite diameter (D) and surface area.

Catalyst	D(A°)	Surface Area (m^2/g)
Fresh $2\%Pt/SiO_2$	391	5.90
Fresh $2\%Pt/2\%La_2O_3/SiO_2$	< 10	>233
Fresh $2\%Pt/5\%La_2O_3/SiO_2$	< 10	>233
Tested $2\%Pt/SiO_2$	590	3.90
Tested $2\%Pt/2\%La_2O_3/SiO_2$	52.1	44.7
Tested $2\%Pt/5\%La_2O_3/SiO_2$	38.4	60.7
Tested $2\%Pd/SiO_2$	110	37.8
Tested $2\%Pd/5\%La_2O_3/SiO_2$	99.1	42.0

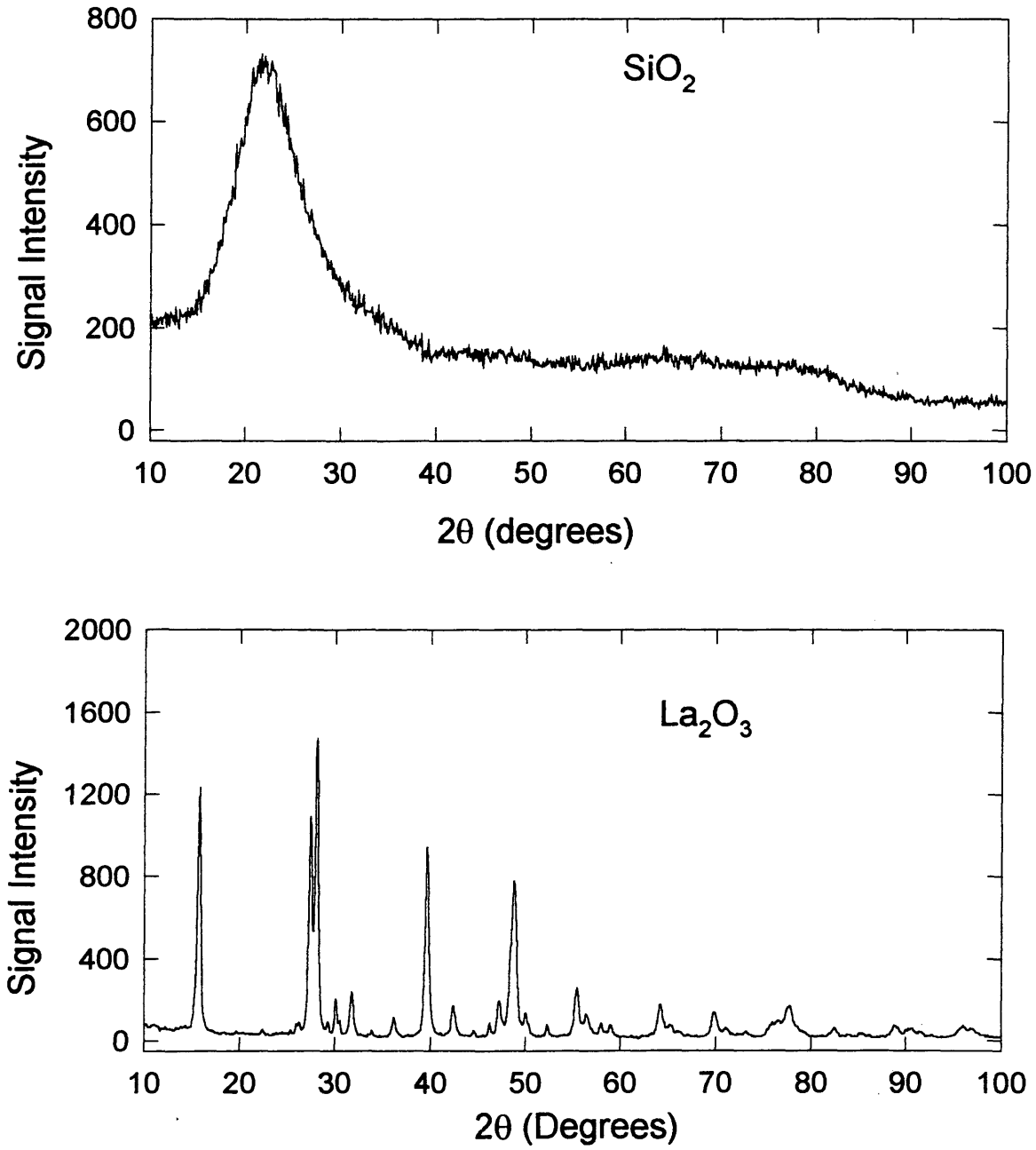

Figure 36. XRD spectra of silica and lanthana.

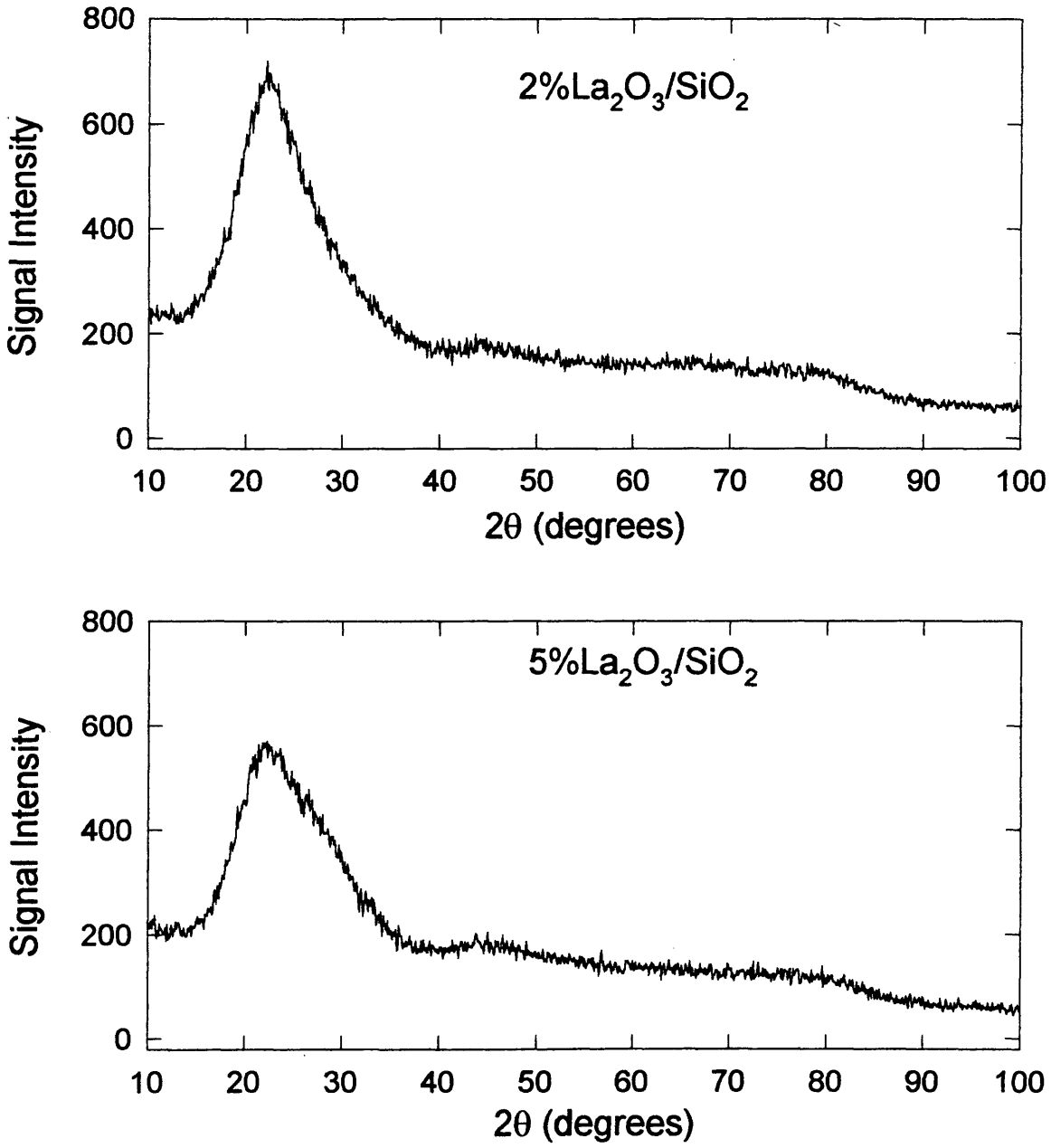

Figure 37. XRD spectra of $2\%La_2O_3/SiO_2$ and $5\%La_2O_3/SiO_2$.

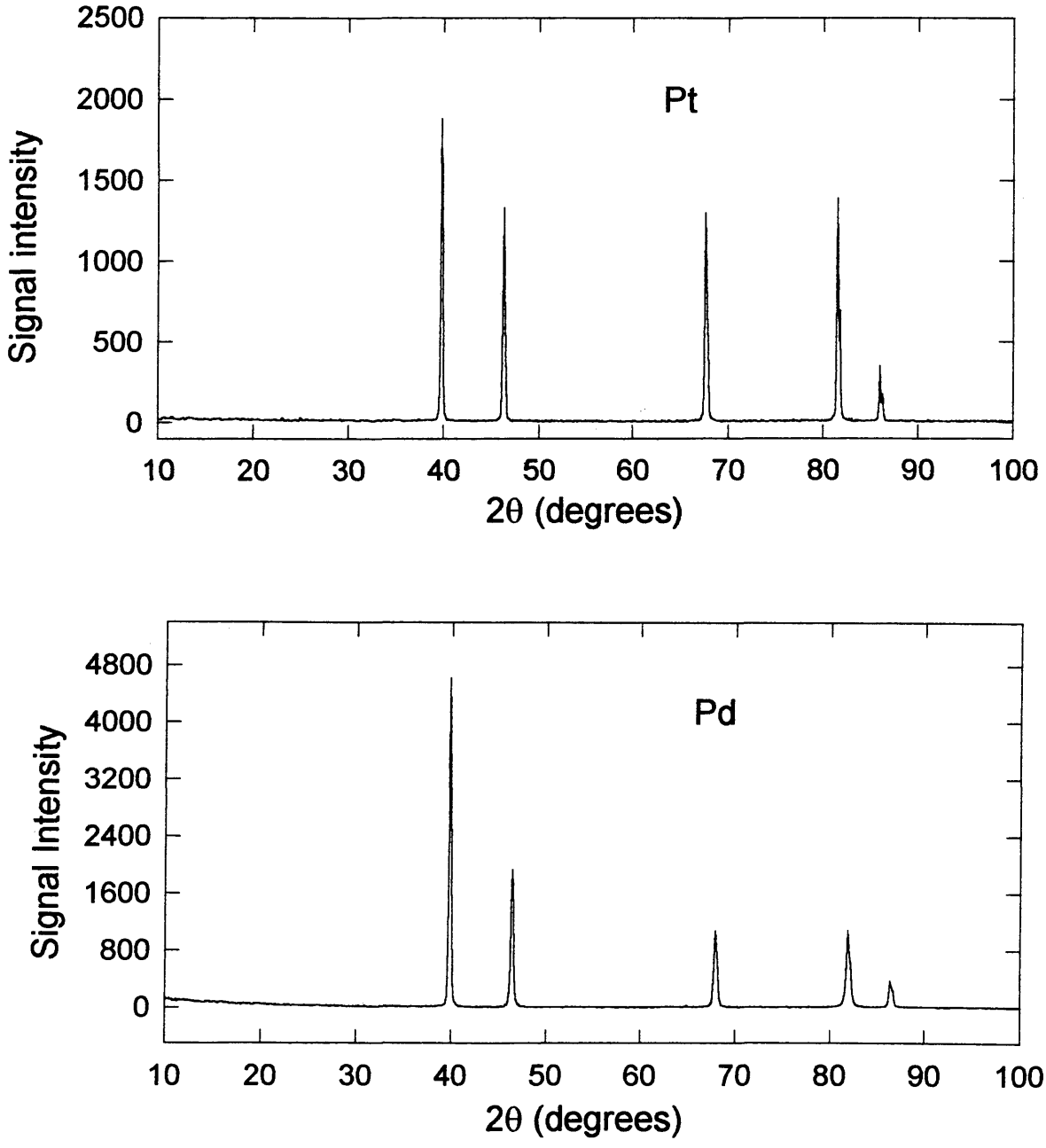

Figure 38. XRD spectra of platinum gauze and palladium powder.

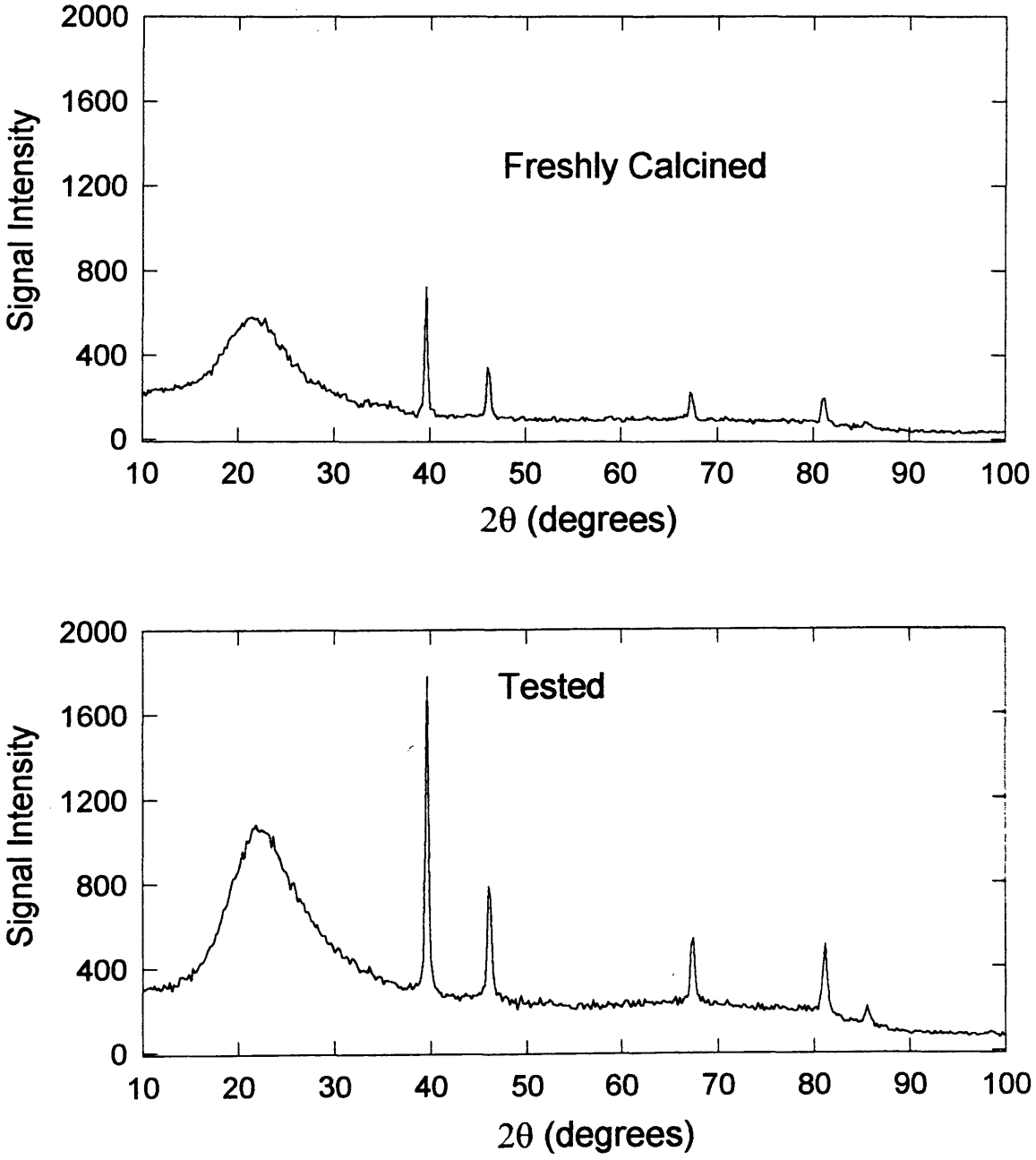

Figure 39. XRD spectra of freshly calcined and tested 2%Pt/SiO_2.

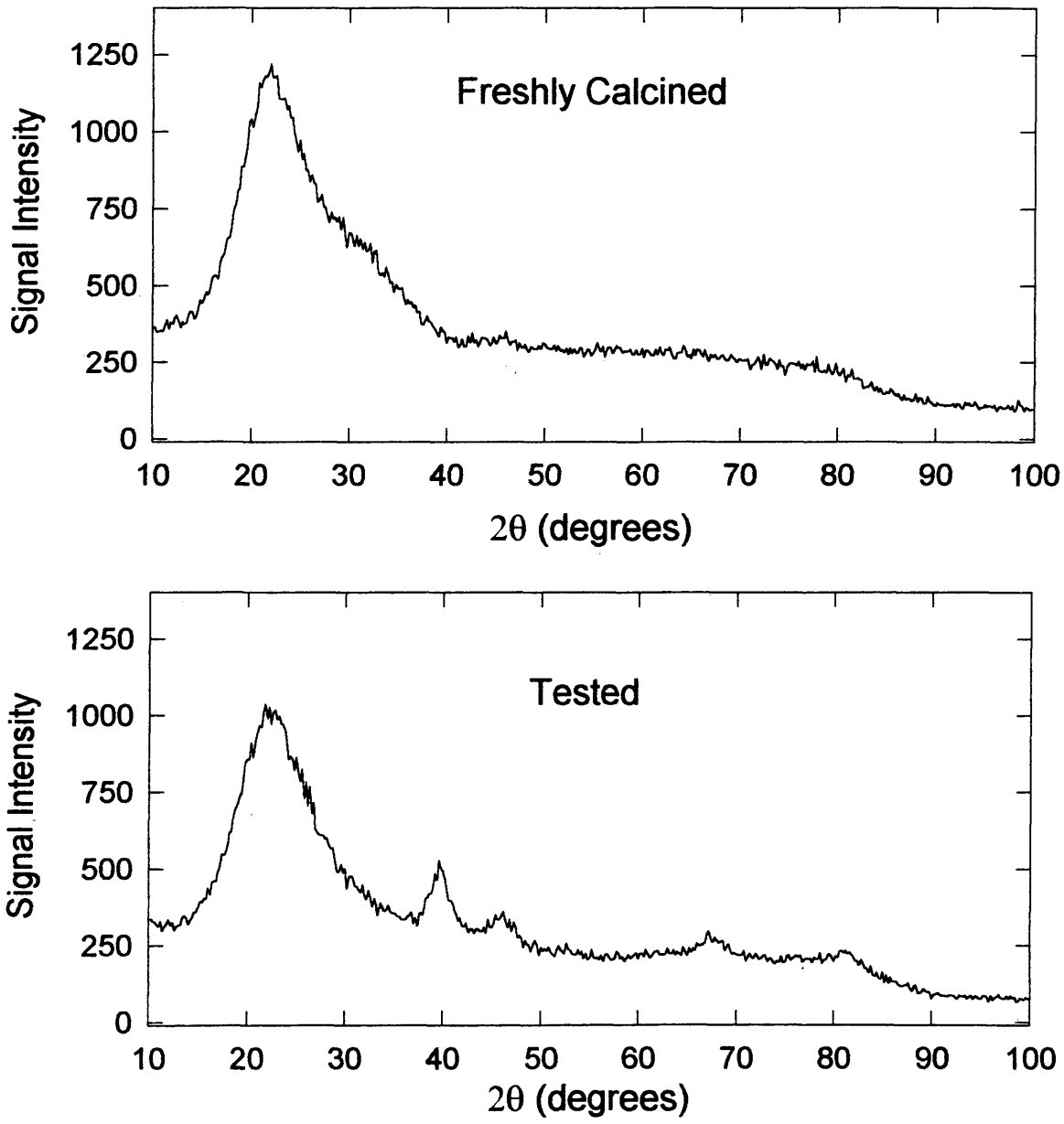

Figure 40. XRD spectra of freshly calcined and tested 2%Pt/2%La_2O_3/SiO_2.

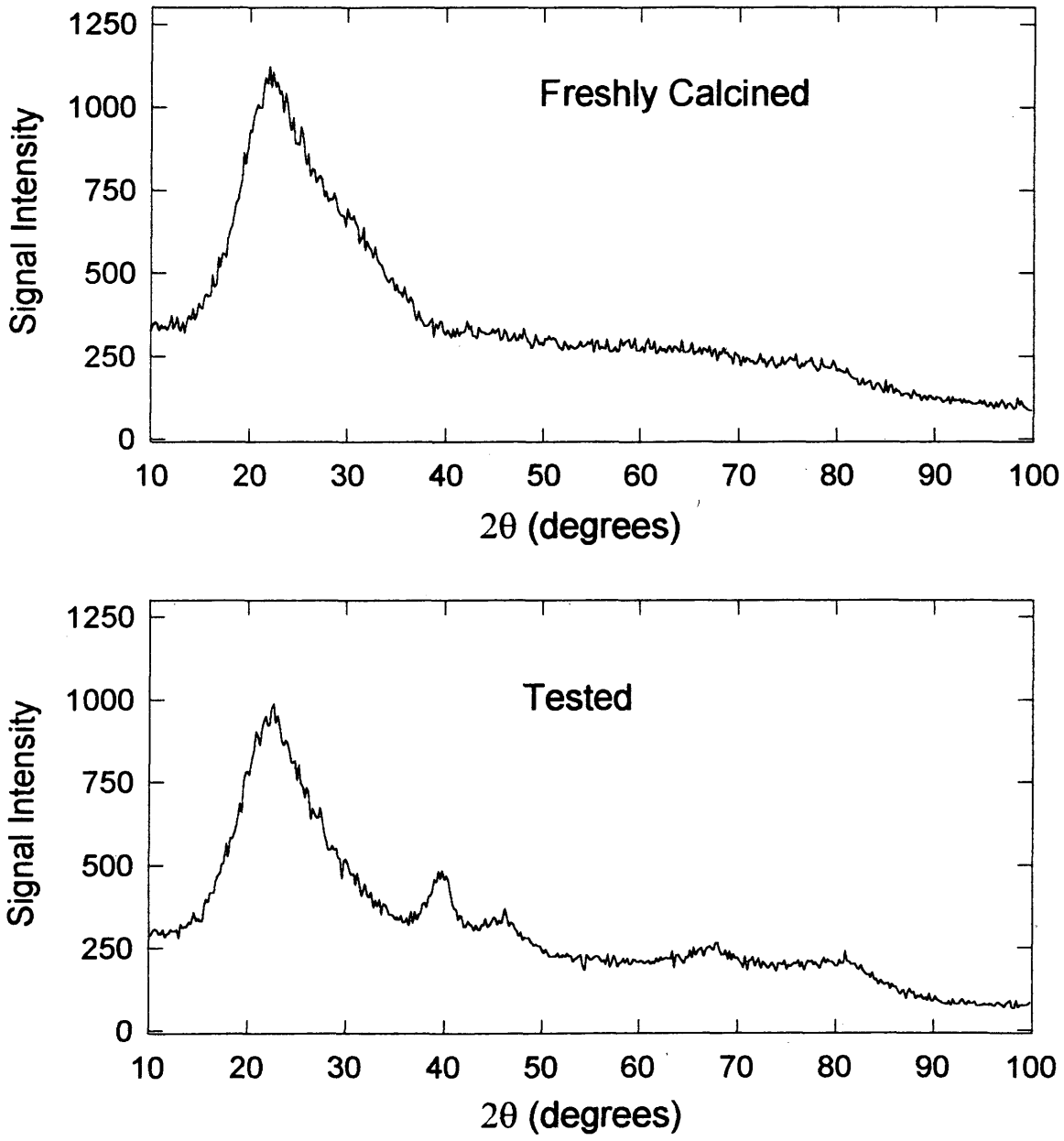

Figure 41. XRD spectra of freshly calcined and tested 2%Pt/5%La_2O_3/SiO_2.

a.

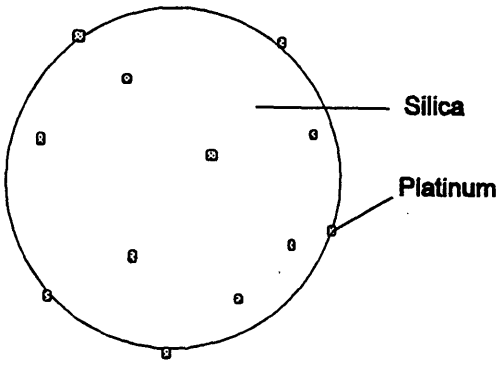

b.

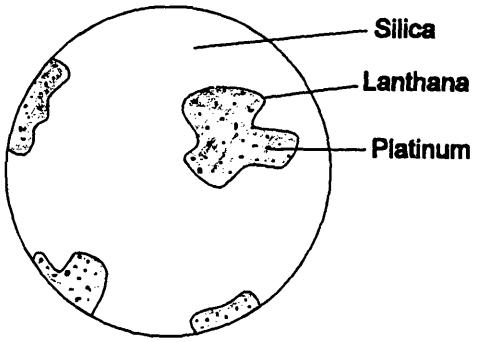

Figure 42. a. A proposed surface picture of 2%Pt//SiO_2 and
b. a proposed surface picture of 2%Pt/5%La_2O_3/SiO_2.

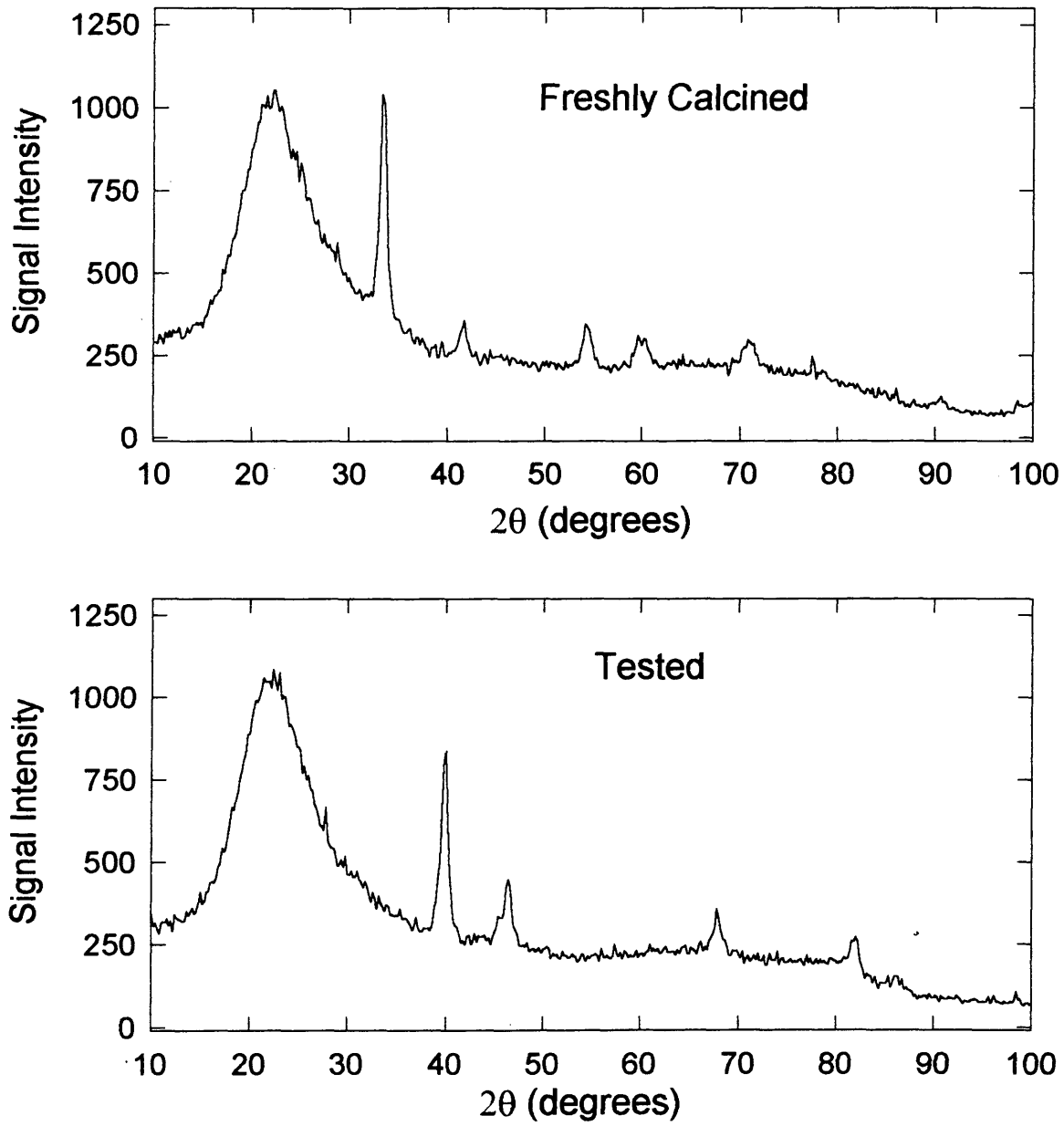

Figure 43. XRD spectra of freshly calcined and tested 2%Pd/SiO_2.

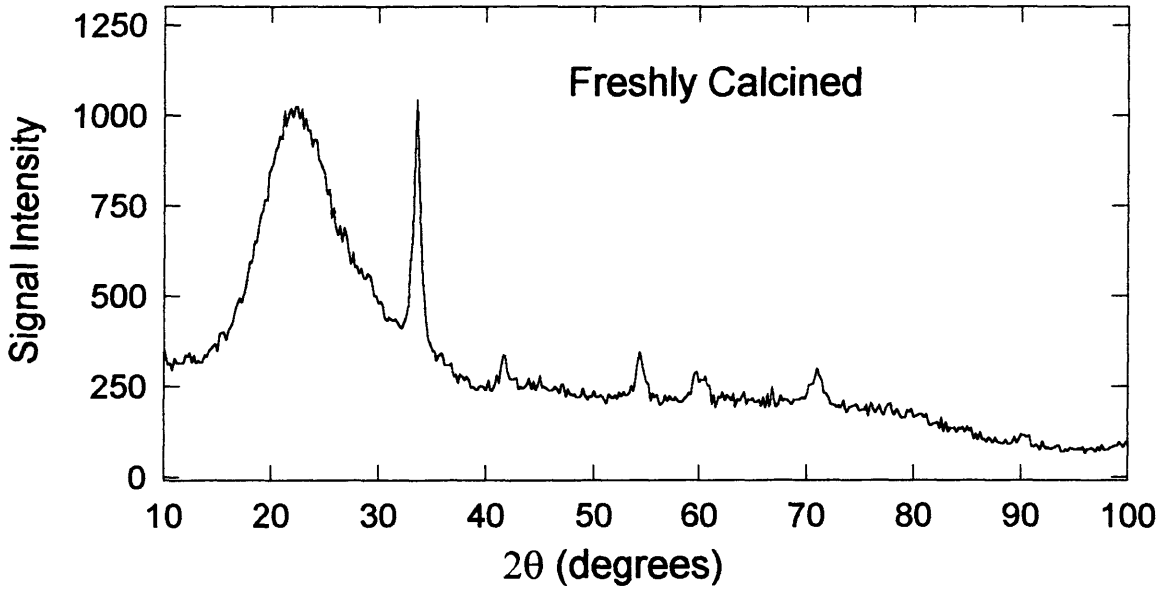

Figure 44. XRD spectra of freshly calcined 2%Pd/2%La_2O_3/SiO_2.

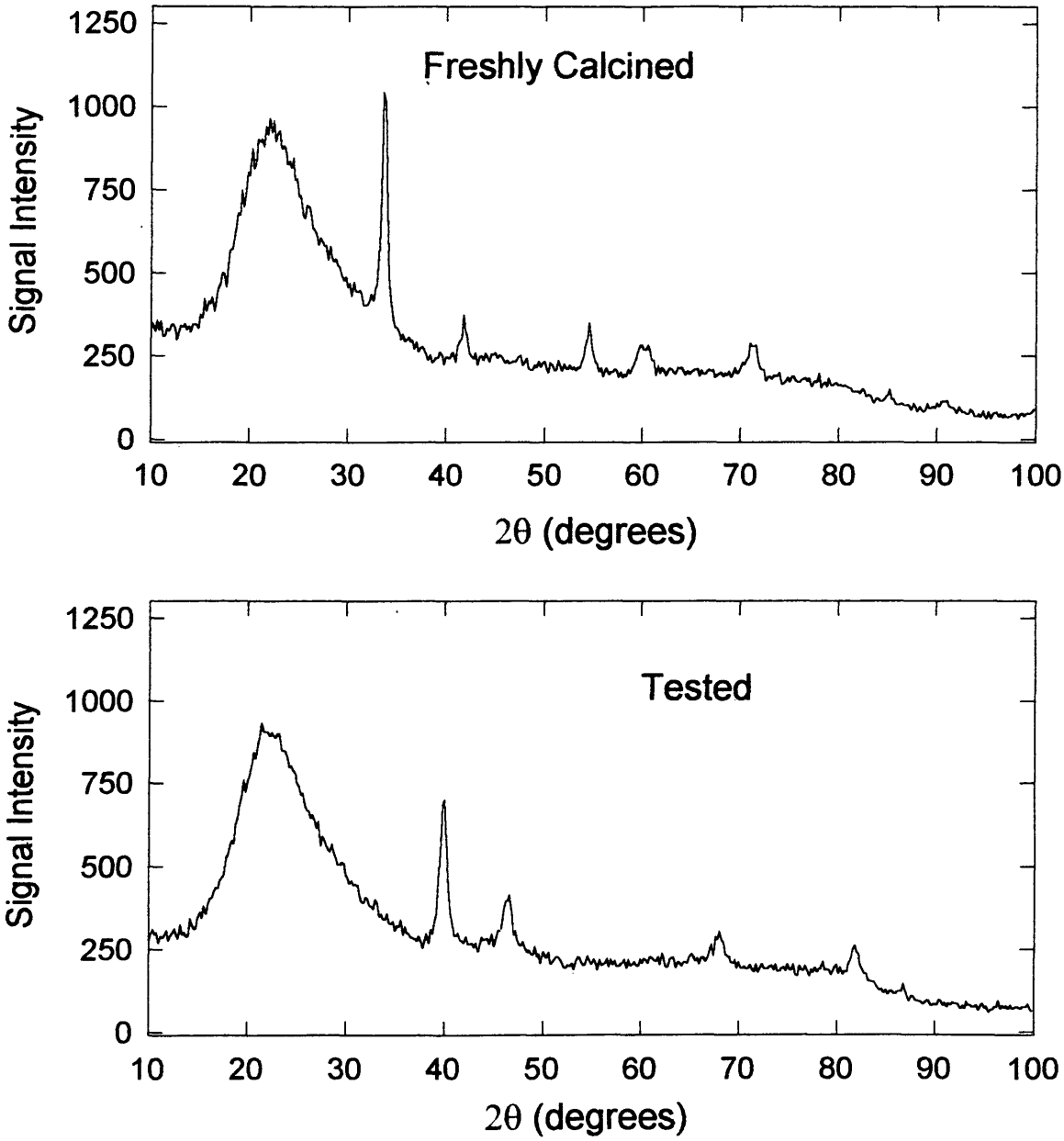

Figure 45. XRD spectra of freshly calcined and tested 2%Pd/5%La_2O_3/SiO_2.

5.6 Catalyst Characterization by X-ray Photoelectron Spectroscopy

X-ray photoelectron spectroscopy (XPS) was used to determine the oxidation state of platinum on the lanthana modified and unmodified silica supports. A survey scan of the freshly calcined 2%Pt/SiO_2 and 2%Pt/5%La_2O_3/SiO_2 catalysts are shown in ***Figures 45 a*** and ***45 b***. Lanthana does appear as a surface species in the modified catalyst. A high resolution scan of the platinum signal in 2%Pt/SiO_2 shows a presence of one doublet at 73 and 77 while in 2%Pt/5%La_2O_3/SiO_2 catalyst shows the presence of two doublets at 74.18 and 77.58, and at 75.98 and 79.38 eV instead of the expected doublet at 73 and 77 eV, see ***Figure 46 a*** and ***46 b***. The additional doublet could be caused by differential charging of the surface during analysis, but none of the other elements show this phenomenon, therefore differential charging was eliminated as the cause. The second set of doublets may correspond to platinum oxide or platinum metal cluster which does not behave as a metal.

In summary, lanthana was identified as a surface species and platinum exists in both the metal and metal oxide phase on a freshly calcined catalyst.

a.

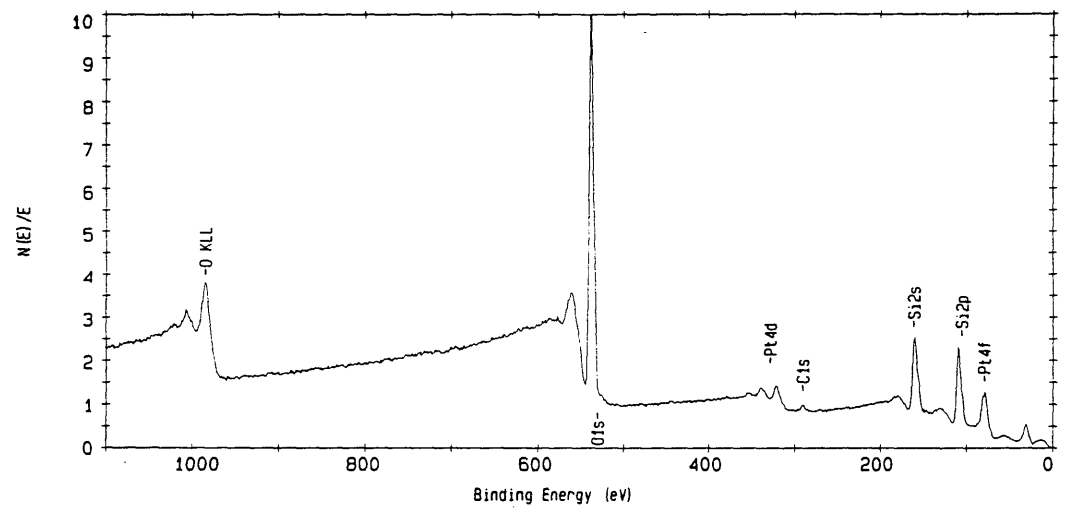

b.

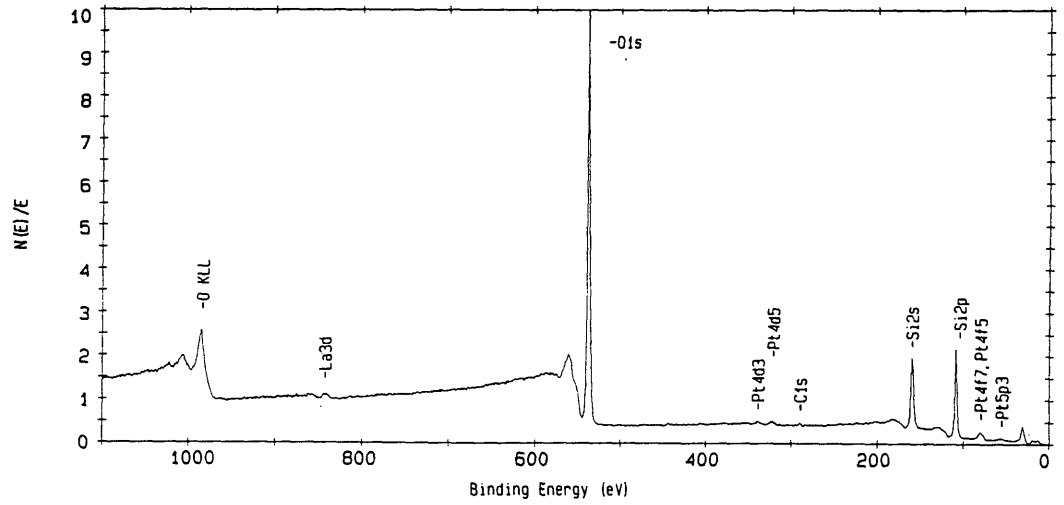

Figure 46. XPS Survey scan of (a) 2%Pt/SiO_2 and (b) 2%Pt/5%La_2O_3/SiO_2.

a.

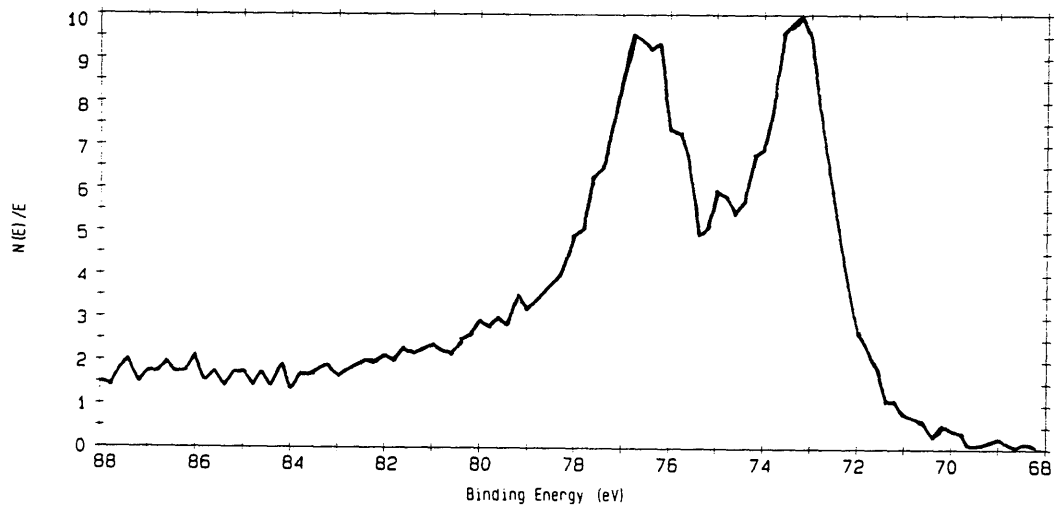

b..

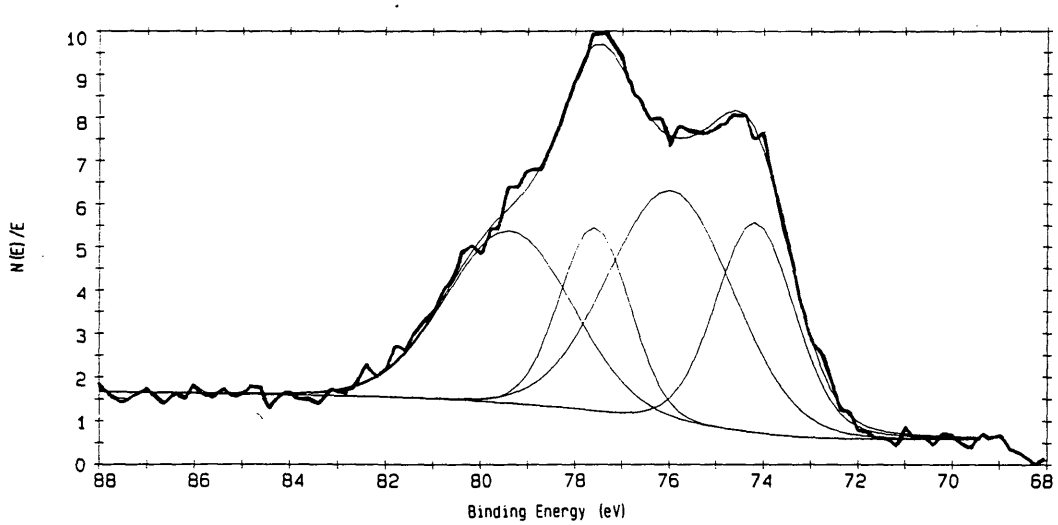

Figure 47. XPS high resolution scan of (a) 2%Pt/SiO_2 and (b) 2%Pt/5%La_2O_3/SiO_2.

Chapter 6
CONCLUSIONS

7.1 Thermodynamic Feasibility of Ethanol Decomposition

Thermodynamic calculations using ASPEN PLUS software show ethanol decomposition to be favorable over the temperature range of 100 to 1000°C. In the 100 to 500°C range, methane and carbon dioxide are the dominant products, while carbon monoxide, hydrogen and methane predominate in the 700 to 1000°C range. For automotive applications, the lower temperature range is desirable and the equilibrium products are acceptable for cold-start applications.

7.2 Catalyst Development

The catalysts showed maximum activity (99-100%) and selectivity (92-96%) at 400°C. The predominant products were hydrogen, carbon monoxide, methane and acetaldehyde, with trace amount of carbon dioxide, ethylene, and ethane. The reaction was far from the predicted thermodynamic equilibrium, suggesting that ethanol dehydrogenation and acetaldehyde decomposition were the kinetically favored reactions in the presence of these catalysts. The water-gas shift and methanation reactions were kinetically limited under these

conditions. The catalyst activity and selectivity were acceptable for on-board cold start applications from 300 to 400°C. A gradual deactivation of the Pt/SiO_2 catalyst was observed in this temperature range, and rapid deactivation occurred for all catalysts at 500°C. Although the catalysts using the lanthana modified silica supports ($Pt/La_2O_3/SiO_2$) showed no sign of deactivation over the 3 hour test period at 400°C, it is likely occurring at a slower rate than the unmodified catalyst. The catalyst deactivation is caused by coke formation, where ethylene, carbon monoxide and possibly acetaldehyde are the coke precursors. The catalyst deactivation problem makes the ethanol decomposition reaction an unlikely candidate for on-board cold start applications. A successful catalyst for this process must not produce ethylene and must be able to remove surface carbon at a reasonable rate.

7.3 Platinum Catalysts Using Modified Silica Supports

The platinum catalysts using lanthana-modified silica supports show a dramatic improvement in metal dispersion and consequently a corresponding improvement in catalyst activity. This was explained in terms of a strong metal support interaction between the platinum metal and the lanthana surface coating. This was supported by XRD and XPS analysis of the catalyst samples. Although the lanthana modified catalysts may not exhibit sufficient selectivity for the on-board cold start applications, they may be valuable materials for other catalytic reactions.

Chapter 7
RECOMMENDATIONS FOR FUTURE STUDY

1. In this study, the basicity of the catalyst support was not measured. It is recommended that the support basicity be determined in order to determine the effect of basicity on metal dispersion. Furthermore, since the dehydration of ethanol still occurred using the lanthanum-modified supports, a technique such as ammonia temperature-programmed desorption (NH_3 TPD) should be used to determine the degree of acidity remaining on the modified supports.
2. In this study, the conclusion about metal dispersion on the support was made based on the XRD results. It is recommended that another technique such as chemisorption be employed to confirm this hypothesis. In addition, using high resolution transmission electron microscopy (HRTEM) can provide more information about metal crystallite structure and the nature of the interaction with the modified support.
3. From the XRD analysis, there was an evidence of the strong metal-support interaction between platinum and lanthana-modified silica. It is recommended that the activity of the modified and unmodified

catalysts be compared with variation of metal surface area. If an interaction exists, the expected linear relationship between the catalyst activity and the metal surface area of the modified and unmodified catalysts will have the same slope but different activity values. The modified catalyst should have the higher activity level.

4. To substantiate the postulation that coking is a cause of catalyst deactivation, one should try burning off the surface carbon on the deactivated catalysts. If the activity can be recovered, coke formation can be concluded to be a major cause of deactivation.
5. Because coke formation results in catalyst deactivation, it is recommended that coking mechanism be studied by two experiments. First, a more complete study of acetaldehyde decomposition in a flow of hydrogen should be conducted since acetaldehyde is an intermediate in the ethanol decomposition. This will lead to the conclusion whether or not acetaldehyde is a cause of coking. Second, carbon monoxide or ethylene feed is applied to the reactor system to determine a degree of coking for each species.
6. During the catalyst evaluations, a large amount of carbon monoxide was generated without catalyst deactivation. If coke is formed from carbon monoxide disproportionation, it must be removed quickly to maintain the activity. The mechanism and kinetics of coke formation and removal is also recommended for future study.

REFERENCES CITED

Castiglioni, J., Kieffer, R., Botana, F.J., Calvino, J.J., Rodriguez-Izquierdo, Vidal, H. 1992. Catalytic Behavior and Surface Properties of Supported Lanthana. J. Alloys and Compounds 180 : 295-301.

Chen, Jr. J., Winograd, N. 1992. Methanolic C-O Bond Activation on Pd(111): A Coverage-Dependent Reaction. J. Am. Chem. Soc. 114 : 2722-2723.

Cullity, B. D., 1978. Elements of X-ray Diffraction, Addison-Wesley Publishing Company, Inc. : 284.

Davidson, J. M., Doraiswamy, L. K. Kulkarni, B. D. Shirridan, C. M. 1987. Catalytic Conversion of Ethanol to Synthesis Gas. Recent Trends. Chem. React. Eng. 2(1): 106-115.

Davis, J. L., Barteau, M.A. 1987. Decarbonylation and Decomposition Pathways of Alcohols on Pd(111). Surf. Sci. 187 : 387-406.

Davis, J. L.; Barteau, M. A. 1990. Spectroscopic Identification of Alkoxide, Aldehyde, and Acyl Intermediates in Alcohol Decomposition on Pd(111). Surf. Sci. 235 : 235-248.

Diddams, P. 1992. Inorganic Supports and Catalysts-An Overview", Solid Supports and Catalysts in Organic Synthesis Smith, K. (Editor). Ellis Horwood Limited.

Gates, S.M., Russell, J.N., Yates, J.T.,Jr. 1986. Bond Activation Sequence Observed in the Chemisorption and Surface Reaction of Ethanol on Ni(111). Surf. Sci. 171 : 111-134.

Guo, X., Xu, Y., Zhai, R., Zhu, K., Huang, J. 1988. Effect between Adspecies on TPD Spectra of Methanol on SiO_2-Supported Pd-Catalyst. Pure & Appl. Chem. 60(8) : 1307-1314.

Iler, R. K. 1979. The Chemistry of Silica, Solubility, Polymerization Colloid, and Surface Properties, and Biochemistry . 57-62.

Jeziorowski, H., Knozinger, H., Meye, W., and Muller, H.D. 1973. H-Bonding on Solid Oxide Surfaces. J. Chem. Soc., Faraday I. 10 : 1744.

Levis, J. R., Zhicheng, J, Winograd, N. 1989. Thermal Decomposition of CH_3OH Adsorbed on Pd(111): A New Reaction Pathway Involving CH_3 Formation. J. Am. Chem. Soc. 111: 4605.

Logsdon, B.W. 1989. The Development and Characterization of Methanol Decomposition Catalysts. Ph.D.Thesis. Colorado School of Mines T-3629.

Metcalfe, A. and Shankar, S.U. 1978. Infrared Studies of Ethanol Adsorbed on Porous Glass. J. Chem. Soc., Faraday Trans.1. 74 (8): 1945-1952.

Mokwa, W., Kohl, D., Heiland, G. 1982. Decomposition of Ethanol and Acetaldehyde on Clean ZnO Prism and Oxygen Faces. Surf. Sci. 117 : 659-667.

Mokwa, W., Kohl, D., Heiland, G. 1983. Decomposition of Ethanol on Cu-ZnO and Pd-ZnO. Fresenius Z. Anal. Chem. 314: 315-318.

Nuffield, E.W., 1966. X-ray Diffraction Method. John Wiley &Sons, Inc. : 147-149.

Page, J. F. Le, 1987. Applied Heterogeneous Catalysis. Gulf Publishing Company. : 106-122.

Perry, J. A. 1981. Introduction to Analytical gas Chromatography. Marcel Dekker, Inc. : 341-349.

Reid, R. C. Prausnitz, J. M., Poling, B. E. 1987. The Properties of Gases and Liquids. McGraw-Hill, Inc. : 150-152.

Scatterfield, C. N. 1991. Heterogeneous Catalysis in Industrial Practice. 2nd edition. McGraw-Hill, Inc. : 130.

Soma, Y., Onishi, T., Tamaru, K. 1969. Mechanism of Alcohol Decomposition over Alumina. Trans.Faraday Soc. 65 (8): 2215-2223.

Wickham, D.T. 1986. An Investigation of Modified Effects upon the Decomposition of Methanol over Alumina Supported Palladium Catalyst. Ph.D. Thesis. Colorado School of Mines, T-3294.

White, M. G., 1990. Heterogeneous Catalysis, Prentice-Hall Inc., 88.

Xu,Y., Zhu, K., Huang, J., Lin, Z., and Guo, X. 1992. The Promoter Action of Lanthana on Methanol Decomposition on Palladium-Lanthana/Silica Catalysts and The Interaction between Coadsorbed Species Studied by Temperature-Programmed Desorption (TPD). J. Nat. Gas. Chem. 1 (2): 93-105.

APPENDIX 1

DETAILS OF A PROGRAM WRITTEN FOR THERMODYNAMIC CALCULATIONS

Program for ethanol decomposition and dehydration

This program was written in BASIC language. The theory and data bank are based on Reid et al. (1987). The program is listed as followed:

```
10   CLEAR : CLS
20   PRINT "This program provides a calculation of"
30   PRINT "  1. Enthalpy of formation"
40   PRINT "  2. Gibbs free energy"
50   PRINT "  3. Equilibrium constant"
60   PRINT "The system varies temperature at a constant pressure 1 atm."
70   PRINT "                                "
80   PRINT "Reference: The Properties of Gases and Liquids, Robert C.Reid,
           John M. Prausnitz"
90   PRINT "        , Bruce E. Poling,TP242.R4, 1987,
                    Page 150-152 and 656-690."
100   PRINT " "
110   PRINT "Select temperature in Kelvin"
120   INPUT "T(K)  =  "; T
130   CLS
140   PRINT "                    At 298 K"
150  PRINT " DATA BANK FOR 1) Ethanol, 2) Carbon monoxide,
                                  3) Methane, 4) Hydrogen,"
160  PRINT "             5) Ethylene, 6) Diethyl ether, 7) Water"
170  DIM CA(7), CB(7), CC(7), CD(7), HF(7), GF(7), H(7), G(7), SF(7), S(7)
180  CA(1) = 9.014: CB(1) = .2141: CC(1) = -.0000839: CD(1) = 1.373E-09:
```

```
      HF(1) = -235000!: GF(1) = -168400!
190   CA(2) = 30.87: CB(2) = -.01285: CC(2) = 2.789E-05:
      CD(2) = -1.272E-08: HF(2) = -110600!: GF(2) = -137400!
200   CA(3) = 19.25: CB(3) = .05213: CC(3) = 1.197E-05:
      CD(3) = -1.132E-08: HF(3) = -74900!: GF(3) = -50870!
210   CA(4) = 27.14: CB(4) = .009274: CC(4) = -1.381E-05:
      CD(4) = 7.645E-09: HF(4) = 0: GF(4) = 0
220   CA(5) = 3.806: CB(5) = .1566: CC(5) = -8.348E-05:
      CD(5) = 1.755E-08: HF(5) = 52340!: GF(5) = 68160!
230   CA(6) = 21.42: CB(6) = .3359: CC(6) = -.0001035:
      CD(6) = -9.357E-09: HF(6) = -252400!: GF(6) = -122400!
240   CA(7) = 32.24: CB(7) = .001924: CC(7) = 1.055E-05:
      CD(7) = -3.596E-09: HF(7) = -242000!: GF(7) = -228800!
250   N = 1
260   H(N) = (HF(N) + CA(N) * (T - 298.15) + CB(N) * (T ^ 2 - 298.15 ^ 2) / 2 +
            CC(N) *(T ^ 3 - 298.15 ^ 3) / 3 + CD(N) * (T ^ 4 - 298.15 ^ 4) / 4) /
            (1000 * 4.18)
270   SF(N) = (GF(N) - HF(N)) / (-298.15)
280   S(N) = (SF(N) + CA(N) * (LOG(T / 298.15)) + CB(N) * (T - 298.15) +
            CC(N) * (T ^  2 - 298.15 ^ 2) / 2 + CD(N) * (T ^ 3 - 298.15 ^ 3) / 3) /
            (1000 * 4.18)
290   G(N) = (H(N) - T * S(N))
300   PRINT N; ")", "H = "; H(N); "kcal/mole", "G = "; G(N); "kcal/mole"
310   N = N + 1
320   IF N < 8 GOTO 210
330   PRINT "There are 3 reaction in this program."
```

```
340  PRINT "1. Ethanol decomposition to carbon monoxide,
                    methane and hydrogen"
350  PRINT "2. Ethanol dehydration to ethylene and water"
360  PRINT "3. Ethanol dehydration to diethyl ether and water"
370  DIM D(3), K(3), HR(3)
380  HR(1) = H(2) + H(3) + H(4) - H(1)
390  HR(2) = H(5) + H(7) - H(1)
400  HR(3) = H(6) + H(7) - 2 * H(1)
410  D(1) = G(2) + G(3) + G(4) - G(1)
420  D(2) = G(5) + G(7) - G(1)
430  D(3) = G(6) + G(7) - 2 * G(1)
440   N = 1
450  K(N) = -D(N) * 4.18 * 1000 / (8.314 * T * 2.303)
460  PRINT "RXN    Delta H kcal/mole", "Delta G kcal/mole", "log K"
470  PRINT N; "  "; HR(N), D(N), K(N)
480  N = N + 1
490  IF N < 4 GOTO 430
500  PRINT "Do you want to calculate other temperature? (Yes = 1,No = 2)"
510  INPUT N
520  IF N = 1 GOTO 60
530  IF N > 1 GOTO 4000
540 END
```

APPENDIX 2
WEIGHT RESPONSE FACTOR

Weight Response Factor Determination

The Perkin Elmer Sigma 3B gas chromatograph using Porapak N was programmed to separate H_2, CO, CH_4, CO_2, C_2H_4, C_2H_6, C_2H_2, H_2O, CH_3CHO, CH_3CH_2OH. To relate area percent to weight percent in an analysis, the gas chromatograph was calibrated with gas and liquid mixtures having known concentrations of the expected components.

Weight response factor (WRF) of component A is calculated by the following equation:

$$\text{WRF A} = \frac{\text{Weight Percent of A}}{\text{Area Percent of A}}$$

In the analysis, the weight percent of a component can be determined by multiplying WRF to area percent:

$$\text{Weight Percent of A} = \text{WRF A x Area Percent A}$$

Then, the mole percent of component A can be determined by

$$\text{Mole Percent of A} = \frac{\text{Wt\% A/MW A}}{(\text{Wt\% A/MW A}) + (\text{Wt\% B/MW B}) + (\text{Wt\% C/MW C}) + \ldots}$$

where Wt% A (or B, C, ...) = weight percent of A (or B, C, ...)
MW A (or B, C, ...) = molecular weight of A (or B, C, ...)

Retention time and weight response factor of expected components in catalyst evaluation are listed in table 5.

Table A2. Retention times and weight response factors (WRF) of gas and liquid standards.

Compound	Retention time (min)	WRF
Hydrogen (H_2)	0.68	23.81
Carbon monoxide (CO)	0.80	0.95
Methane (CH_4)	1.00	0.69
Carbon dioxide (CO_2)	1.80	1.32
Ethylene (C_2H_4)	2.14	0.85
Ethane (C_2H_6)	2.17	0.83
Acetylene (C_2H_4)	2.54	0.94
Water (H_2O)	5.80	0.72
Acetaldehyde (C_2H_4O)	8.23	2.43
Ethanol (C_2H_6O)	14.00	0.91

APPENDIX 3
TEMPERATURE PROFILE IN THE REACTOR

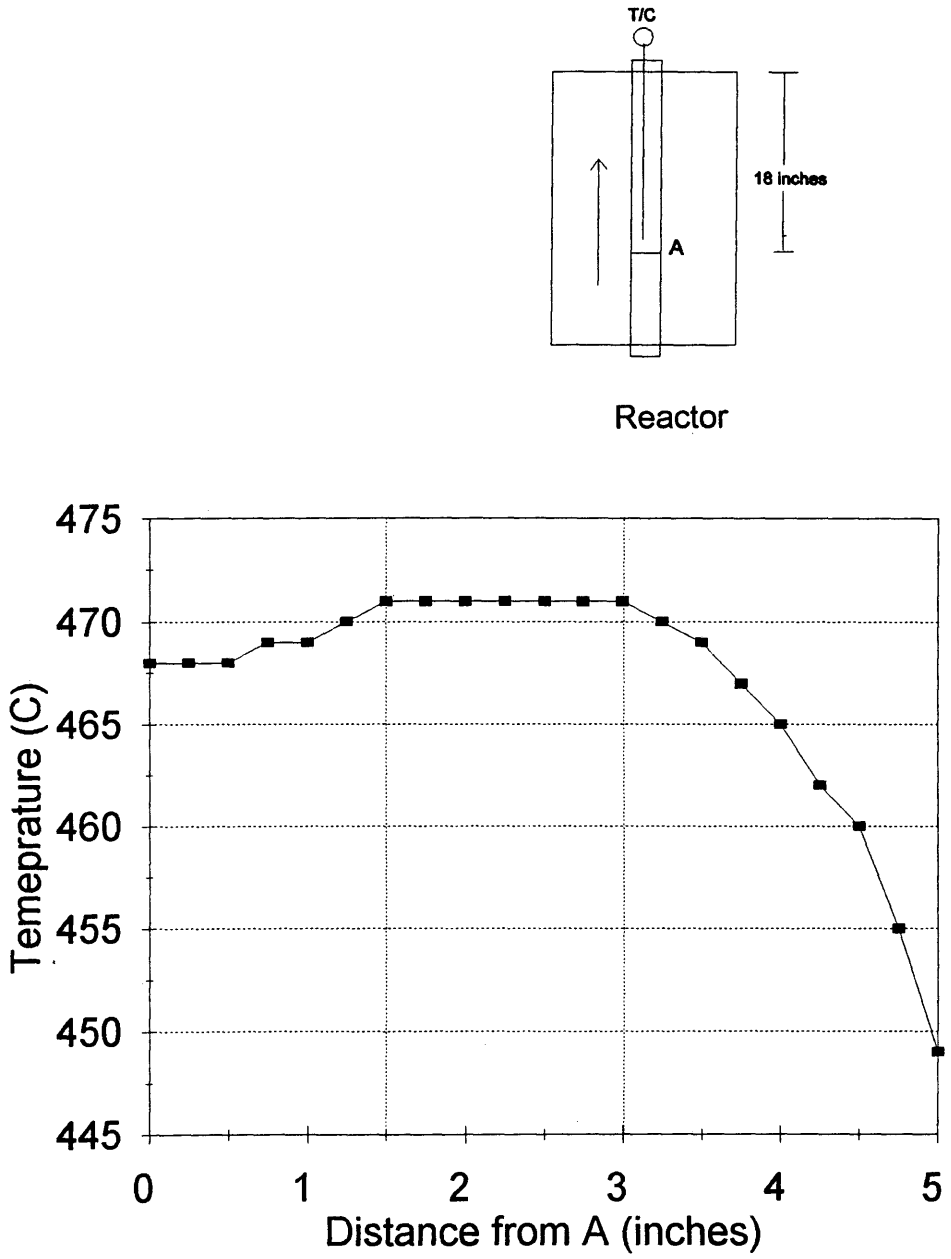

Figure 48. Temperature profile inside the reactor.

APPENDIX 4
ANALYTICAL RESULTS

Table A4-1. Ethanol reactions on 2%Pt/SiO_2

Tested Material: 0.400 g. of 2%Pt/SiO_2 and 1.000 g. quartz chips

Feed Composition: 1.5 cc/hr ethanol + 20 cc/min helium

Space Velocity: 3.5 hr^{-1}

Temp (C)	Mole % of component									selectivity %	activity %
	H2	CO	CH4	CO2	C2H4	C2H6	H2O	C2H4O	C2H6O		
200	4.46	0.22	0.20	0.00	0.00	0.00	0.00	4.25	90.87	4.92	1.81
200	4.35	0.24	0.22	0.00	0.00	0.00	0.00	4.11	90.09	5.52	1.73
200	4.42	0.24	0.22	0.00	0.00	0.00	0.00	4.18	90.95	5.43	1.78
200	4.59	0.24	0.23	0.00	0.00	0.00	0.00	4.35	90.58	5.23	1.73
200	4.66	0.25	0.23	0.00	0.00	0.00	0.00	4.42	90.45	5.35	2.43
200	4.61	0.25	0.23	0.00	0.00	0.00	0.00	4.36	90.46	5.42	1.71
average	4.52	0.24	0.22	0.00	0.00	0.00	0.00	4.28	90.57	5.31	1.87
300	29.42	9.85	9.93	0.05	0.05	0.05	0.10	19.45	31.12	33.45	36.08
300	29.08	8.97	9.03	0.04	0.04	0.05	0.09	20.00	32.70	30.82	33.88
300	28.45	8.08	8.13	0.04	0.04	0.04	0.08	20.28	34.88	28.37	31.25
300	28.56	8.01	8.06	0.04	0.04	0.04	0.08	20.46	34.72	28.02	31.63
300	28.76	8.01	8.06	0.04	0.04	0.04	0.08	20.66	34.28	27.82	31.84
300	28.87	7.81	7.85	0.04	0.04	0.04	0.09	20.97	34.29	27.02	31.60
average	28.86	8.46	8.51	0.04	0.04	0.04	0.09	20.30	33.67	29.25	32.71
400	33.49	32.60	33.10	0.26	0.00	0.15	0.15	0.24	0.00	98.05	100.00
400	33.53	32.49	32.97	0.24	0.05	0.12	0.17	0.44	0.00	97.45	100.00
400	33.61	32.34	32.82	0.22	0.05	0.11	0.16	0.69	0.00	96.80	100.00
400	33.51	32.17	32.27	0.20	0.06	0.09	0.15	1.15	0.38	95.54	98.70
400	33.62	31.94	32.40	0.20	0.07	0.08	0.15	1.14	0.41	95.54	98.60
400	33.68	31.71	32.14	0.19	0.07	0.08	0.15	1.47	0.52	94.60	98.29
400	33.69	31.64	32.05	0.19	0.08	0.07	0.15	1.57	0.57	94.31	98.15
average	33.59	32.13	32.54	0.21	0.05	0.10	0.15	0.96	0.27	96.04	99.11
500	12.83	1.02	0.79	0.08	3.54	0.19	3.73	11.62	66.20	6.20	12.64
500	10.26	0.69	0.49	0.06	3.23	0.16	3.39	9.41	72.32	5.09	9.93
500	8.84	0.54	0.37	0.00	2.96	0.13	3.09	8.17	75.89	4.58	8.31
500	8.23	0.50	0.33	0.00	2.93	0.13	3.06	7.61	77.22	4.48	7.90
500	7.56	0.44	0.28	0.00	2.78	0.12	2.90	7.00	78.92	4.26	7.16
500	7.12	0.32	0.25	0.00	2.78	0.12	2.89	6.68	79.83	3.23	6.88
average	9.14	0.59	0.42	0.02	3.04	0.14	3.18	8.42	75.06	4.64	8.80
300	0.82	0.00	0.00	0.00	0.00	0.00	0.00	0.82	98.37	0.00	0.41
300	0.63	0.00	0.00	0.00	0.00	0.00	0.00	0.63	98.74	0.00	0.38
300	0.57	0.00	0.00	0.00	0.00	0.00	0.00	0.57	98.87	0.00	0.30
300	0.58	0.00	0.00	0.00	0.00	0.00	0.00	0.58	98.84	0.00	0.25
average	0.65	0.00	0.00	0.00	0.00	0.00	0.00	0.65	98.71	0.00	0.34

Comment : After testing, the catalyst color was darker than at the beginning of the test, suggesting that coking occurred.

Table A4-2. Ethanol reactions on 2%Pt/2%La_2O_3/SiO_2

Tested Material: 0.400 g. of 2%Pt/2%La_2O_3/SiO_2 and 1.000 g. quartz chips

Feed Composition: 1.5 cc/hr ethanol + 20 cc/min helium

Space Velocity: 3.5 hr^{-1}

Temp	Mole % of component									selectivity	activity
(C)	H2	CO	CH4	CO2	C2H4	C2H6	H2O	C2H4O	C2H6O	%	%
200	19.40	1.06	0.97	0.00	0.00	0.00	0.00	18.34	60.23	5.46	11.73
200	19.66	1.12	1.04	0.00	0.00	0.00	0.00	18.54	59.64	5.70	12.00
200	19.99	1.17	1.08	0.00	0.00	0.00	0.00	18.82	58.95	5.85	12.27
200	19.53	1.10	1.03	0.00	0.00	0.00	0.00	18.43	59.91	5.63	11.78
200	19.39	1.08	1.01	0.00	0.00	0.00	0.00	18.31	60.22	5.57	11.63
200	19.65	1.10	1.02	0.00	0.00	0.00	0.00	18.55	59.69	5.60	12.21
200	19.33	1.06	0.98	0.00	0.00	0.00	0.00	18.27	60.35	5.48	11.47
average	19.56	1.10	1.02	0.00	0.00	0.00	0.00	18.47	59.86	5.61	11.87
300	36.74	21.92	22.07	0.24	0.06	0.42	0.48	14.57	3.59	58.91	89.11
300	37.45	19.67	19.82	0.22	0.06	0.37	0.42	17.63	4.36	51.83	86.53
300	37.78	18.43	18.58	0.21	0.05	0.33	0.39	19.21	5.02	48.21	84.43
300	37.98	17.71	17.86	0.20	0.05	0.32	0.37	20.13	5.38	46.11	83.26
300	37.99	17.72	17.87	0.21	0.05	0.32	0.37	20.12	5.36	46.12	83.30
300	38.13	17.10	17.25	0.20	0.05	0.30	0.35	20.89	5.73	44.37	82.16
average	37.68	18.76	18.91	0.21	0.05	0.34	0.40	18.76	4.91	49.26	84.80
400	34.03	29.96	34.03	1.98	0.00	0.00	0.00	0.00	0.00	93.80	100.00
400	33.86	30.61	33.86	1.68	0.00	0.00	0.00	0.00	0.00	94.80	100.00
400	33.39	30.62	33.39	1.50	0.55	0.00	0.55	0.00	0.00	93.73	100.00
400	33.35	30.79	33.35	1.43	0.54	0.00	0.54	0.00	0.00	93.99	100.00
400	33.35	30.80	33.35	1.42	0.54	0.00	0.54	0.00	0.00	94.02	100.00
400	33.30	31.05	33.30	1.30	0.53	0.00	0.53	0.00	0.00	94.43	100.00
400	33.31	31.02	33.31	1.32	0.52	0.00	0.52	0.00	0.00	94.40	100.00
average	33.51	30.69	33.51	1.52	0.38	0.00	0.38	0.00	0.00	94.17	100.00
500	33.34	10.35	6.65	2.47	3.67	0.41	4.07	22.58	16.47	26.22	62.63
500	28.95	4.89	2.97	1.44	4.45	0.44	4.89	23.62	28.35	14.04	46.91
500	25.58	3.20	1.93	1.00	4.51	0.46	4.97	21.92	36.42	10.29	36.29
500	23.97	2.57	1.57	0.84	4.77	0.50	5.27	20.90	39.61	8.69	33.75
500	22.71	2.17	1.34	0.73	4.95	0.53	5.49	20.01	42.07	7.64	31.27
500	21.68	1.84	1.16	0.63	4.99	0.55	5.55	19.28	44.31	6.74	29.20
average	26.04	4.17	2.60	1.19	4.56	0.48	5.04	21.39	34.54	12.27	40.01
300	0.95	0.00	0.00	0.00	0.00	0.00	0.00	0.95	98.09	0.00	0.95
300	1.24	0.00	0.00	0.00	0.00	0.00	0.00	1.24	97.52	0.00	1.24
300	1.40	0.00	0.00	0.00	0.00	0.00	0.00	1.40	97.20	0.00	1.40
300	1.49	0.00	0.00	0.00	0.00	0.00	0.00	1.49	97.02	0.00	1.49
average	1.27	0.00	0.00	0.00	0.00	0.00	0.00	1.27	97.46	0.00	1.27

Comment : After testing, the catalyst color was darker than at the beginning of the test, suggesting that coking occurred.

Table A4-3. Ethanol reactions on 2%Pt/5%La_2O_3/SiO_2

Tested Material: 0.400 g. of 2%Pt/5%La_2O_3/SiO_2 and 1.000 g. quartz chips

Feed Composition: 1.5 cc/hr ethanol + 20 cc/min helium

Space Velocity: 3.5 hr^{-1}

Temp	Mole % of component									selectivity	activity
(C)	H2	CO	CH4	CO2	C2H4	C2H6	H2O	C2H4O	C2H6O	%	%
200	20.35	1.30	1.17	0.00	0.00	0.00	0.00	19.05	57.06	6.39	15.00
200	21.14	1.41	1.28	0.00	0.00	0.00	0.00	19.73	55.40	6.67	16.09
200	21.18	1.41	1.29	0.00	0.00	0.00	0.00	19.78	55.36	6.65	16.00
200	21.31	1.41	1.28	0.00	0.00	0.00	0.00	19.90	55.06	6.62	16.29
200	20.88	1.34	1.23	0.00	0.00	0.00	0.00	19.55	55.98	6.41	15.63
200	20.90	1.32	1.22	0.00	0.00	0.00	0.00	19.57	56.03	6.32	15.46
average	20.96	1.37	1.25	0.00	0.00	0.00	0.00	19.60	55.82	6.51	15.75
300	35.79	24.49	24.38	0.41	0.06	0.47	0.53	11.30	2.58	66.68	92.37
300	36.69	21.93	21.84	0.38	0.06	0.41	0.47	14.76	3.45	58.42	89.62
300	36.93	21.07	20.98	0.38	0.06	0.39	0.45	15.85	3.88	55.81	88.33
300	37.21	20.33	20.25	0.37	0.06	0.38	0.44	16.88	4.09	53.47	87.57
300	37.28	19.95	19.89	0.37	0.06	0.37	0.42	17.32	4.34	52.40	86.74
300	37.42	19.60	19.55	0.37	0.05	0.36	0.42	17.81	4.42	51.32	86.49
average	36.89	21.23	21.15	0.38	0.06	0.40	0.46	15.65	3.79	56.35	88.52
400	33.77	28.79	33.77	2.41	0.00	0.63	0.63	0.00	0.00	90.45	100.00
400	33.59	29.50	33.59	2.11	0.00	0.60	0.60	0.00	0.00	91.59	100.00
400	33.50	29.86	33.50	1.96	0.00	0.59	0.59	0.00	0.00	92.13	100.00
400	33.43	30.15	33.43	1.84	0.00	0.58	0.58	0.00	0.00	92.57	100.00
400	33.42	30.21	33.42	1.81	0.00	0.57	0.57	0.00	0.00	92.70	100.00
400	33.39	30.32	33.39	1.76	0.00	0.57	0.57	0.00	0.00	92.86	100.00
400	33.36	30.43	33.36	1.71	0.00	0.57	0.57	0.00	0.00	93.03	100.00
average	33.49	29.89	33.49	1.94	0.00	0.59	0.59	0.00	0.00	92.19	100.00
500	32.38	21.02	32.38	5.45	0.04	1.39	1.43	0.00	0.00	75.34	100.00
500	32.02	14.60	10.09	5.80	4.28	0.62	4.91	16.79	10.88	34.69	76.66
500	27.20	6.49	4.31	3.57	5.94	0.60	6.54	20.11	25.23	17.68	55.27
500	24.54	4.25	2.79	2.53	6.44	0.67	7.11	19.63	32.04	12.68	47.08
500	22.87	3.20	2.12	2.01	6.77	0.72	7.49	18.95	35.88	10.11	42.91
500	21.86	2.61	1.76	1.71	7.06	0.78	7.84	18.47	37.92	8.52	40.84
500	19.32	1.92	1.3	1.27	6.86	0.74	7.6	16.67	44.33	6.99	34.33
average	25.74	7.73	7.82	3.19	5.34	0.79	6.13	15.80	26.61	23.72	56.73
300	0.55	0.00	0.00	0.00	0.00	0.00	0.00	0.55	98.90	0.00	0.55
300	0.66	0.00	0.00	0.00	0.00	0.00	0.00	0.66	98.68	0.00	0.66
300	0.78	0.00	0.00	0.00	0.00	0.00	0.00	0.78	98.43	0.00	0.78
average	0.66	0.00	0.00	0.00	0.00	0.00	0.00	0.66	98.67	0.00	0.66

Comment : After testing, the catalyst color was darker than at the beginning of the test, suggesting that coking occurred.

Table A4-4. Ethanol reactions on 2%Pd/SiO_2

Tested Material: 0.400 g. of 2%Pd/SiO_2 and 1.000 g. quartz chips

Feed Composition: 1.5 cc/hr ethanol + 20 cc/min helium

Space Velocity: 3.5 hr^{-1}

Temp	Mole % of component									selectivity	activity
(C)	H2	CO	CH4	CO2	C2H4	C2H6	H2O	C2H4O	C2H6O	%	%
200	1.92	0.62	0.48	0.00	0.00	0.00	0.00	1.34	95.60	31.63	1.03
200	2.09	0.69	0.51	0.00	0.00	0.00	0.00	1.40	95.32	33.01	1.57
200	2.03	0.74	0.51	0.00	0.00	0.00	0.00	1.29	95.43	36.45	1.56
200	1.88	0.71	0.53	0.00	0.00	0.00	0.00	1.17	95.71	37.77	1.46
200	1.75	0.67	0.50	0.00	0.00	0.00	0.00	1.08	96.00	38.29	1.39
average	1.93	0.69	0.51	0.00	0.00	0.00	0.00	1.26	95.61	35.43	1.40
300	12.75	9.64	9.77	0.00	0.00	0.00	0.00	2.98	64.84	76.39	14.22
300	13.19	9.76	9.86	0.00	0.00	0.00	0.00	3.33	63.86	74.56	14.46
300	13.02	9.50	9.60	0.00	0.00	0.00	0.00	3.43	64.45	73.47	14.03
300	13.35	9.57	9.68	0.00	0.00	0.00	0.00	3.67	63.73	72.28	14.31
300	13.62	9.66	9.76	0.00	0.00	0.00	0.00	3.86	63.10	71.45	14.62
300	13.81	9.62	9.72	0.00	0.00	0.00	0.00	4.09	62.76	70.17	14.67
average	13.29	9.63	9.73	0.00	0.00	0.00	0.00	3.56	63.79	73.05	14.39
400	5.60	0.22	0.10	0.00	0.15	0.04	0.19	5.43	88.22	3.77	1.59
400	4.99	0.12	0.06	0.00	0.14	0.04	0.18	4.92	89.51	2.30	1.20
400	4.77	0.12	0.05	0.00	0.14	0.04	0.18	4.69	89.96	2.40	0.99
average	3.94	0.11	0.05	0.00	0.11	0.03	0.14	3.89	91.61	2.12	1.08
300	0.53	0.00	0.00	0.00	0.00	0.00	0.00	0.53	98.74	0.00	0.53

Comment : After testing, the catalyst was darken from coking.

Table A4-5. Ethanol reactions on 2%Pd/5%La_2O_3/SiO_2

Tested Material: 0.400 g. of 2%Pd/5%La_2O_3/SiO_2 and 1.000 g. quartz chips

Feed Composition: 1.5 cc/hr ethanol + 20 cc/min helium

Space Velocity: 3.5 hr^{-1}

Temp	Mole % of component									selectivity	activity
(C)	H2	CO	CH4	CO2	C2H4	C2H6	H2O	C2H4O	C2H6O	%	%
200	1.93	0.67	0.51	0.00	0.00	0.00	0.00	1.43	95.46	31.90	1.61
200	1.90	0.72	0.56	0.00	0.00	0.00	0.00	1.34	95.50	34.95	1.50
200	1.88	0.76	0.58	0.00	0.00	0.00	0.00	1.29	95.38	37.07	1.60
200	1.77	0.73	0.55	0.00	0.00	0.00	0.00	1.22	95.60	37.44	1.48
200	1.71	0.71	0.54	0.00	0.00	0.00	0.00	1.16	95.69	37.97	1.44
200	1.71	0.71	0.54	0.00	0.00	0.00	0.00	1.17	95.65	37.77	1.49
average	1.82	0.72	0.55	0.00	0.00	0.00	0.00	1.27	95.55	36.18	1.52
300	23.29	18.34	18.25	0.00	0.00	0.00	0.00	5.05	35.07	78.41	38.35
300	21.89	16.52	16.33	0.00	0.00	0.00	0.00	5.55	39.70	74.85	33.37
300	21.35	15.74	15.55	0.00	0.00	0.00	0.00	5.80	41.57	73.07	31.64
300	20.45	15.80	14.42	0.00	0.00	0.00	0.00	6.03	43.31	72.38	29.60
300	20.19	14.11	13.73	0.00	0.00	0.00	0.00	6.46	45.52	68.60	28.06
300	19.90	13.41	12.95	0.00	0.00	0.00	0.00	6.95	46.78	65.86	26.90
average	21.18	15.65	15.21	0.00	0.00	0.00	0.00	5.97	41.99	72.20	31.32
400	5.01	0.90	0.29	0.74	0.00	0.00	0.00	4.11	88.94	15.65	4.47
400	3.40	0.55	0.15	0.73	0.00	0.00	0.00	3.23	91.56	12.20	3.34
400	3.00	0.45	0.11	0.71	0.00	0.00	0.00	2.88	92.52	11.14	3.31
400	2.81	0.14	0.10	0.69	0.00	0.00	0.00	2.71	93.52	3.95	2.57
average	3.56	0.51	0.16	0.72	0.00	0.00	0.00	3.23	91.64	10.74	3.42
300	0.52	0.00	0.00	0.00	0.00	0.00	0.00	0.52	98.86	0.00	0.52

Comment : The catalyst color was black after testing and si,ilar in appearance to the tested 2%Pd/SiO2 catalyst. It is the result of catalyst coking.

APPENDIX 5

ESTIMATION OF PERCENT LANTHANA COVERAGE ON SILICA

Estimation of Percent Lanthana Coverage on Silica

Silica surface area	= 300 m^2/g
Lanthana molecular weight	= 325.81
Ionic radii of oxygen	= 1.40 A°
Projection area (πr^2)	= 6.16×10^{-20} m^2/atom
Ionic radii of lanthanum	= 1.16 A°
Projection area	= $4.23 \times 10^{-20} m^2$/atom
Area of La_2O_3	= $(2 \times 4.23 \times 10^{-20}) + (3 \times 6.16 \times 10^{-20})$
	= 26.93×10^{-20} m^2/molecule

1. 2%La_2O_3/SiO_2

2%La_2O_3/SiO_2 100 g contains SiO_2 98 g and La_2O_3 2 g

La_2O_3 2 g	= 3.7×10^{21} molecule
area	= 995.1 m^2
Percent coverage	= 995.1 x 100/(300 x 98)
	= 3.4%

2. 5%La_2O_3/SiO_2

5%La_2O_3/SiO_2 100 g contains SiO_2 95 g and La_2O_3 5 g

La_2O_3 5 g	= 9.2×10^{21} molecule
area	= 2487.7 m^2
Percent coverage	= 2487.7 x 100/(300 x 95)
	= 8.7%